Article

Molecular Engineering of Intensely Near-Infrared Absorbing Excited States in Highly Conjugated Oligo(porphinato)zinc–(Polypyridyl)metal(II) Supermolecules

Timothy V. Duncan, Tomoya Ishizuka, and Michael J. Therien

J. Am. Chem. Soc., **2007**, 129 (31), 9691-9703• DOI: 10.1021/ja0707512 • Publication Date (Web): 13 July 2007

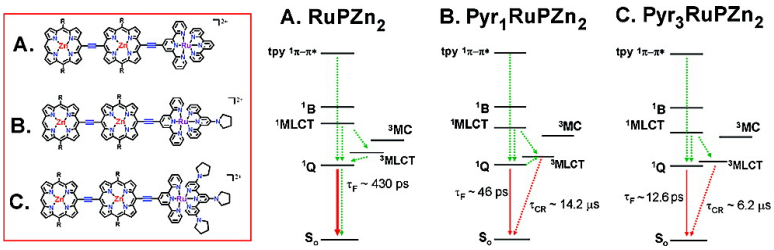

More About This Article

Additional resources and features associated with this article are available within the HTML version:

- Supporting Information
- Links to the 3 articles that cite this article, as of the time of this article download
- Access to high resolution figures
- Links to articles and content related to this article
- Copyright permission to reproduce figures and/or text from this article

View the Full Text HTML

J|A|C|S
ARTICLES
Published on Web 07/13/2007

Molecular Engineering of Intensely Near-Infrared Absorbing Excited States in Highly Conjugated Oligo(porphinato)zinc−(Polypyridyl)metal(II) Supermolecules

Timothy V. Duncan, Tomoya Ishizuka, and Michael J. Therien*

Contribution from the Department of Chemistry, University of Pennsylvania, Philadelphia, Pennsylvania 19104-6323

Received February 2, 2007; E-mail: therien@sas.upenn.edu

Abstract: A new series of chromophores, **MPZn$_n$**, which combine ethyne-bridged bis(terpyridyl)metal(II)−(porphinato)zinc(II) (**MPZn**) and oligomeric, ethyne-bridged (porphinato)zinc(II) (**PZn$_n$**) architectures, have been synthesized and characterized, along with a series of derivatives bearing pyrrolidinyl electron-releasing groups on the ancillary terpyridine units (**Pyr$_m$MPZn$_n$**). Cyclic voltammetric studies, as well as NMR, electronic absorption, fluorescence, and femtosecond pump−probe transient absorption spectroscopies, have been employed to study the ground- and excited-state properties of these unusual chromophores. All of these species possess intensely absorbing excited states having large spectral bandwidth that penetrate deep in the near-infrared (NIR) energy regime. Electronic structural variation of the molecular framework shows that the excited-state absorption maximum can be extensively modulated [$\lambda_{max}(T_1 \rightarrow T_n)$] (880 nm $< \lambda_{max} <$ 1126 nm), while concomitantly maintaining impressively large $T_1 \rightarrow T_n$ absorption manifold spectral bandwidth (full width at half-maximum, fwhm, ∼2000−2500 cm^{-1}). Furthermore, these studies enable correlation of supermolecular electronic structure with the magnitude of the excited-state lifetime (τ_{es}) and demonstrate that this parameter can be modulated over 4 orders of magnitude (∼1 ns $< \tau_{es} <$ 45 μs). Terpyridyl pyrrolidinyl substituents can be utilized to destabilize terpyridyl ligand π^* energy levels and diminish the $E_{1/2}$ ($M^{3+/2+}$) value of the bis(terpyridyl)metal(II) center: such perturbations determine the relative energies of the **PZn$_n$**-derived $^1\pi-\pi^*$ and bis(terpyridyl)metal(II) charge-transfer states and establish whether the T_1-state wave functions of **MPZn$_n$** and **Pyr$_m$MPZn$_n$** species manifest the extensive electronic delocalization and charge-separated (CS) features characteristic of long-lived triplet states that absorb strongly in the NIR.

Introduction

The efficiency of nonlinear optical (NLO) materials for long-wavelength reverse saturable absorption (RSA)[1−4] and optical power limiting (OPL)[4−6] applications hinges in large part upon engineering strongly absorbing excited states having long lifetimes. Because of this requirement, chromophores which populate an excited triplet state after photoexcitation are often utilized, due to the fact that ground-state recovery from excited triplet states is usually retarded by spin-conservation selection rules. In the visible region (400 $< \lambda <$ 800 nm), OPL materials based upon phthalocyanine,[5,7−10] porphyrin,[11,12] fullerene/nanotube,[6,13−16] and other[17−20] motifs have already been identified; however, examples of chromophores suitable for such NLO applications in the near-infrared (NIR) are limited. This derives from the fact that as chromophore optical band gaps shift to progressively lower energies, intersystem crossing (ISC) generally becomes inefficient due to the increased rates of competing internal conversion processes.[21−24] Furthermore, even in species which possess near-unity ISC quantum yields (such as those

(1) Nalwa, H. S.; Shirk, J. S. In *Phthalocyanines: Properties and Applications*; Leznoff, C. C., Lever, A. B. P., Eds.; VCH: Weinheim, Germany, 1996; p 79.
(2) Perry, J. W. In *Nonlinear Optics of Organic Molecules and Polymers*; Nalwa, H. S., Miyata, S., Eds.; CRC Press: Boca Raton, FL, 1997; p 813.
(3) Harter, D. J.; Shand, M. L.; Band, Y. B. *J. Appl. Phys.* **1984**, *56*, 865−868.
(4) Tutt, L. W.; Boggess, T. F. *Prog. Quantum Electron.* **1993**, *17*, 299−338.
(5) Chen, Y.; Hanack, M.; Araki, Y.; Ito, O. *Chem. Soc. Rev.* **2005**, *34*, 517−529.
(6) Innocenzi, P.; Lebeau, B. *J. Mater. Chem.* **2005**, *15*, 3821−3831.
(7) Perry, J. W.; Mansour, K.; Lee, I.-Y. S.; Wu, X. L.; Bedworth, P. V.; Chen, C.-T.; Ng, D.; Marder, S. R.; Miles, P.; Wada, T.; Tian, M.; Sasabe, H. *Science* **1996**, *273*, 1533−1536.
(8) de la Torre, G.; Vázquez, P.; Agulló-López, F.; Torres, T. *Chem. Rev.* **2004**, *104*, 3723−3750.
(9) Shirk, J. S.; Pong, R. G. S.; Bartoli, F. J.; Snow, A. W. *Appl. Phys. Lett.* **1993**, *63*, 1880−1882.
(10) Nitschke, C.; O'Flaherty, S. M.; Kröll, M.; Blau, W. J. *J. Phys. Chem. B* **2004**, *108*, 1287−1295.
(11) Chen, P.; Tomov, I. V.; Dvornikov, A. S.; Nakashima, M.; Roach, J. F.; Alabran, D. M.; Rentzepis, P. M. *J. Phys. Chem.* **1996**, *100*, 17507−17512.
(12) Su, W.; Cooper, T. M.; Brant, M. C. *Chem. Mater.* **1998**, *10*, 1212−1213.
(13) Tutt, L. W.; Kost, A. *Nature* **1992**, *356*, 225−226.
(14) Brusatin, G.; Signorini, R. *J. Mater. Chem.* **2002**, *12*, 1964−1977.
(15) Goh, H. W.; Goh, S. H.; Xu, G. Q.; Lee, K. Y.; Yang, G. Y.; Lee, Y. W.; Zhang, W.-D. *J. Phys. Chem. B* **2003**, *107*, 6056−6062.
(16) Chin, K. C.; Gohel, A.; Chen, W. Z.; Elim, H. I.; Ji, W.; Chong, G. L.; Sow, C. H.; Wee, A. T. S. *Chem. Phys. Lett.* **2005**, *409*, 85−88.
(17) Liu, R. S. H.; Asato, A. E. *J. Photochem. Photobiol., C* **2003**, *4*, 179−194.
(18) Zhang, J.; Sun, X.; Smith, K. M.; Visser, F.; Carpenter, P.; Barron, G.; Peng, Y.; Robins, M. J.; Baldwin, S. A.; Young, J. D.; Cass, C. E. *Biochemistry* **2006**, *45*, 1087−1098.
(19) Sun, W.; Dai, Q.; Worden, J. G.; Huo, Q. *J. Phys. Chem. B* **2005**, *109*, 20854−20857.
(20) Shang, X.; Zhang, G.; Liu, Y.; Tang, G.; Chen, W. J. *J. Phys. Chem. A* **1998**, *102*, 7487−7497.

Scheme 1. Design Strategy of Highly Conjugated Hybrid Bis(terpyridyl)metal(II)−(Porphinato)zinc(II) **MPZn$_n$** Chromophores (n = Total Number of Conjugated **PZn** Units)[a]

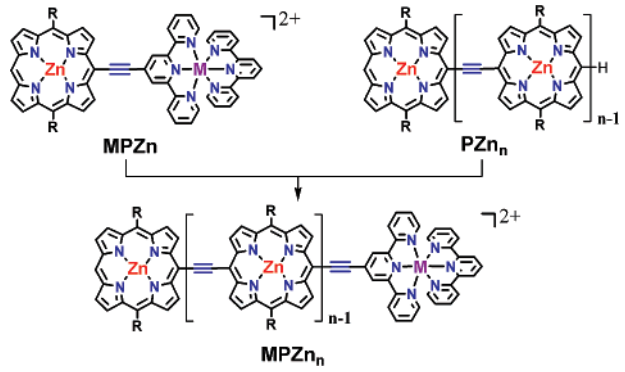

[a] R = 2′,6′-bis(3,3-dimethyl-1-butyloxy)phenyl.

which utilize heavy atoms), excited triplet-state molar absorptivities beyond 800 nm are often small,[21] due to challenges associated with engineering extensive excited-triplet wave function delocalization in π-conjugated systems.[25−35] For these reasons, the realization of OPL chromophores which are both optically active in the NIR and possess long-lived, strongly absorbing excited-states remains an unmet molecular engineering goal.

This laboratory has described the design, synthesis, spectroscopy, and excited-state dynamics of two heretofore unrelated series of highly conjugated chromophores (Scheme 1): (i) multimeric (porphinato)zinc(II) arrays that feature ethyne-bridged macrocycle-to-macrocycle linkage motifs (**PZn$_n$** structures);[25−28,36−41] (ii) hybrid **MPZn** chromophores incorporating ethyne-linked (porphinato)zinc(II) (**PZn**) and bis(terpyridyl)-metal(II) (**M**; metal = **Ru**, **Os**) subunits.[42,43] In **MPZn** chromophores, **PZn** and (terpyridyl)metal(II) moieties possess a characteristic ethyne-bridged porphyrin *meso*-carbon to terpyridyl 4′-carbon linkage topology (Scheme 1), which has been shown to facilitate efficient excited-state electronic communication between the subunits. Previous work on ethyne-bridged **PZn$_n$** oligomers that feature a *meso*-to-*meso* linkage motif demonstrates that these compounds manifest low-energy Q-state derived $\pi-\pi^*$ excited states that are polarized exclusively along the long molecular axis[25,26,36,37,39−41,44−46] and exhibit intensely absorbing $S_1 \rightarrow S_n$ transitions that extend deep into the NIR energy regime [compound, ($[\lambda_{max}(S_1 \rightarrow S_n)]$, full width at half-maximum, fwhm): **PZn$_2$** (980 nm, 656 cm^{-1}),[39] **PZn$_3$** (1120 nm, 750 cm^{-1}),[41] and **PZn$_5$** (1325 nm, 1980 cm^{-1})][41] in THF solvent. Notably, the excited states of these species (i) relax to their respective electronic ground states on nanosecond (ns) time scales, (ii) display large fluorescence quantum yields, and (iii) manifest modest-to-minimal triplet yields that decrease with increasing conjugation length.[41] In contrast, studies that probe the relaxation dynamics of the low-lying excited states of **MPZn** species show that, within 200 fs following photoexcitation, the initially prepared excited state relaxes to a highly polarized charge-separated (CS) T_1 state[43] that differs in many respects from the MLCT state of conventional (polypyridyl)metal(II) species;[47−51] this **MPZn** CS triplet excited state relaxes nonradiatively via charge recombination dynamics on timescales ranging from 0.86 μs (**OsPZn**) to 44 μs (**RuPZn**).[43] While the primary excited-state relaxation pathway of **MPZn** species is related to that for charge-recombination (CR) deactivation of classical (polypyridyl)metal(II) charge-transfer (CT) states, because **MPZn** $T_1 \rightarrow T_n$ manifold transitions involve states having substantial CS character, these absorptions feature considerable **PZn** π-system oscillator strength. **MPZn** species thus exhibit intense NIR excited-state absorption bands, with large excited-state molar extinction coefficients $\epsilon_e[\lambda_{max}(T_1 \rightarrow T_n)]$ ranging from ∼30 000 to ∼100 000 M^{-1} cm^{-1}, and impressive bandwidths [compound, ($[\lambda_{max}(T_1 \rightarrow T_n)]$, fwhm): **RuPZn** (884 nm, ∼2730 cm^{-1}); **OsPZn** (964 nm, >2015 cm^{-1}).[43]

This work motivated the engineering of a new class of compounds (**MPZn$_n$** chromophores, Scheme 1) that exhibits the combined properties of these two benchmark, highly conjugated multichromophore motifs: (i) the enormous NIR $T_1 \rightarrow T_n$ transition intensities; (ii) μs excited-state relaxation dynamics of thermally relaxed **MPZn** excited states, with (iii) the tunable excited-state absorption manifolds characteristic of **PZn$_n$** oligomers. Chart 1 highlights **RuPZn$_2$** and **OsPZn$_2$** structures, while Chart 2 describes related **Pyr$_m$RuPZn$_n$** compounds that feature pyrrolidinyl (**Pyr**) substituents that modulate terpyridyl ligand π^* energy levels and diminish the $E_{1/2}(M^{3+/2+})$ value of the bis(terpyridyl)metal(II) center. Herein we discuss the

(21) Turro, N. J. *Modern Molecular Photochemistry*; University Science Books: Sausolito, CA, 1991.
(22) Caspar, J. V.; Kober, E. M.; Sullivan, B. P.; Meyer, T. J. *J. Am. Chem. Soc.* **1982**, *104*, 630−632.
(23) Caspar, J. V.; Meyer, T. J. *J. Phys. Chem.* **1983**, *87*, 952−957.
(24) Englman, R.; Jortner, J. *Mol. Phys.* **1970**, *18*, 145.
(25) Angiolillo, P. J.; Lin, V. S.-Y.; Vanderkooi, J. M.; Therien, M. J. *J. Am. Chem. Soc.* **1995**, *117*, 12514−12527.
(26) Shediac, R.; Gray, M. H. B.; Uyeda, H. T.; Johnson, R. C.; Hupp, J. T.; Angiolillo, P. J.; Therien, M. J. *J. Am. Chem. Soc.* **2000**, *122*, 7017−7033.
(27) Angiolillo, P. J.; Susumu, K.; Uyeda, H. T.; Lin, V. S.-Y.; Shediac, R.; Therien, M. J. *Synth. Met.* **2001**, *116*, 247−253.
(28) Angiolillo, P. J.; Uyeda, H. T.; Duncan, T. V.; Therien, M. J. *J. Phys. Chem. B* **2004**, *108*, 11893−11903.
(29) Piet, J. J.; Taylor, P. N.; Anderson, H. L.; Osuka, A.; Warman, J. M. *J. Am. Chem. Soc.* **2000**, *122*, 1749−1757.
(30) Piet, J. J.; Taylor, P. N.; Wegewijs, B. R.; Anderson, H. L.; Osuka, A.; Warman, J. M. *J. Phys. Chem. B* **2001**, *105*, 97−104.
(31) Swanson, L. S.; Lane, P. A.; Shinar, J.; Wudl, F. *Phys. Rev. B* **1991**, *44*, 10617−10621.
(32) Swanson, L. S.; Shinar, J.; Yoshino, K. *Phys. Rev. Lett.* **1990**, *65*, 1140−1143.
(33) Bennati, M.; Grupp, A.; Mehring, M.; Bäuerle, P. *J. Phys. Chem.* **1996**, *100*, 2849−2853.
(34) Beljonne, D.; Cornil, J.; Friend, R. H.; Janssen, R. A. J.; Brédas, J. L. *J. Am. Chem. Soc.* **1996**, *118*, 6453−6461.
(35) List, E. J. W.; Partee, J.; Shinar, J.; Scherf, U.; Müllen, K.; Zojer, E.; Petritsch, K.; Leising, G.; Graupner, W. *Phys. Rev. B* **2000**, *61*, 10807−10814.
(36) Lin, V. S.-Y.; Di Magno, S. G.; Therien, M. J. *Science* **1994**, *264*, 1105−1111.
(37) Lin, V. S.-Y.; Therien, M. J. *Chem.*—Eur. *J.* **1995**, *1*, 645−651.
(38) Priyadarshy, S.; Therien, M. J.; Beratan, D. N. *J. Am. Chem. Soc.* **1996**, *118*, 1504−1510.
(39) Rubtsov, I. V.; Susumu, K.; Rubtsov, G. I.; Therien, M. J. *J. Am. Chem. Soc.* **2003**, *125*, 2687−2696.
(40) Susumu, K.; Therien, M. J. *J. Am. Chem. Soc.* **2002**, *124*, 8550−8552.
(41) Duncan, T. V.; Susumu, K.; Sinks, L. E.; Therien, M. J. *J. Am. Chem. Soc.* **2006**, *128*, 9000−9001.
(42) Uyeda, H. T.; Zhao, Y. X.; Wostyn, K.; Asselberghs, I.; Clays, K.; Persoons, A.; Therien, M. J. *J. Am. Chem. Soc.* **2002**, *124*, 13806−13813.
(43) Duncan, T. V.; Rubtsov, I. V.; Uyeda, H. T.; Therien, M. J. *J. Am. Chem. Soc.* **2004**, *126*, 9474−9475.
(44) Kumble, R.; Palese, S.; Lin, V. S.-Y.; Therien, M. J.; Hochstrasser, R. M. *J. Am. Chem. Soc.* **1998**, *120*, 11489−11498.
(45) Fletcher, J. T.; Therien, M. J. *Inorg. Chem.* **2002**, *41*, 331−341.
(46) Duncan, T. V.; Wu, S. P.; Therien, M. J. *J. Am. Chem. Soc.* **2006**, *128*, 10423−10435.
(47) Meyer, T. J. *Pure Appl. Chem.* **1986**, *58*, 1193−1206.
(48) Juris, A.; Balzani, V.; Barigelletti, F.; Campagna, S.; Belser, P.; von Zelewsky, A. *Coord. Chem. Rev.* **1988**, *84*, 85−277.
(49) Sauvage, J.-P.; Collin, J.-P.; Chambron, J.-C.; Guillerez, S.; Coudret, C.; Balzani, V.; Barigelletti, F.; De Cola, L.; Flamigni, L. *Chem. Rev.* **1994**, *94*, 993−1019.
(50) Maestri, M.; Armaroli, N.; Balzani, V.; Constable, E. C.; Thompson, A. M. W. C. *Inorg. Chem.* **1995**, *34*, 2759−2767.
(51) Balzani, V.; Bergamini, G.; Marchioni, F.; Ceroni, P. *Coord. Chem. Rev.* **2006**, *250*, 1254−1266.

Chart 1. Structures of **RuPZn$_2$** and **OsPZn$_2$** Compounds

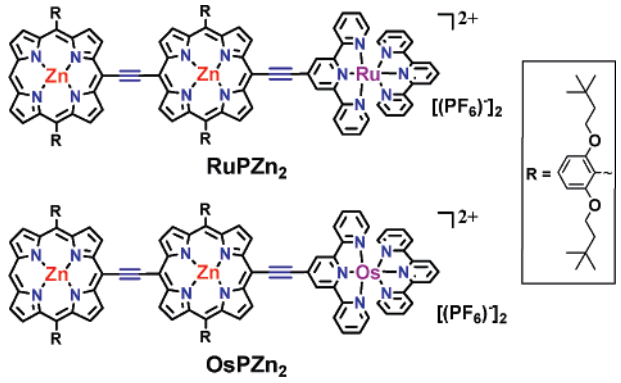

Chart 2. Structures of **Pyr$_m$RuPZn**and **Pyr$_m$RuPZn$_2$** Compounds

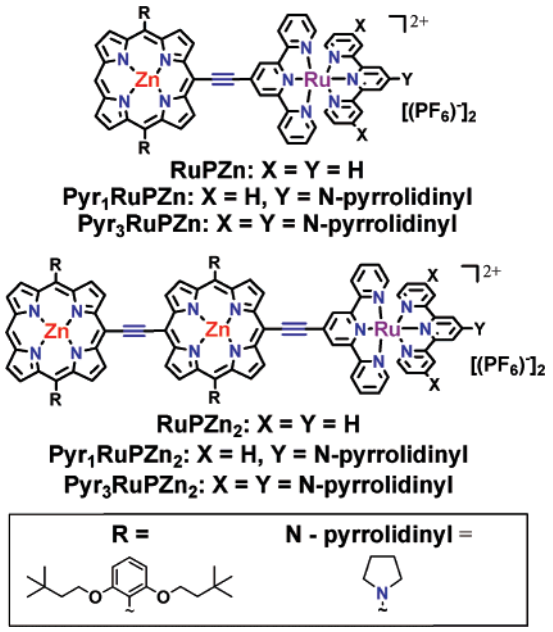

synthesis, electrochemistry, steady-state absorption, and time-resolved transient absorption spectroscopy of these chromophoric species and correlate the structure of these supermolecules with the nature of the initially prepared and thermally relaxed excited sates. These studies show that the T_1-state wave functions of conjugated **MPZn$_n$** chromophores can not only manifest the extensive electronic delocalization and the charge-separated (CS) features characteristic of impressive **MPZn** NIR absorbers but can be engineered to give rise to excited states that provide excellent spectral coverage and possess lifetimes and $T_1 \rightarrow T_n$ absorption maxima that are tunable respectively over wide time and energy domains.

Experimental Section

1. Synthesis and Characterization. A full account of the synthesis and characterization of all new compounds, complete with detailed reaction schemes, is provided in the Supporting Information.

2. Instrumentation. Electronic absorption spectra were recorded on a Shimadzu UV-1700 spectrophotometer, and emission spectra were recorded on a SPEX Fluorolog luminescence spectrometer that utilized a T-channel configuration and PMT/InGaAs/Extended-InGaAs detectors. Emission spectra were corrected using the spectral output of a calibrated light source supplied by the National Bureau of Standards. Low temperature (77 K) spectra were recorded using an optical dewar.

Scheme 2. Syntheses of **RuPZn**, **Pyr$_1$RuPZn**, **Pyr$_3$RuPZn**, **RuPZn$_2$**, **Pyr$_1$RuPZn$_2$**, **Pyr$_3$RuPZn$_2$**, **OsPZn**, and **OsPZn$_2$**[a]

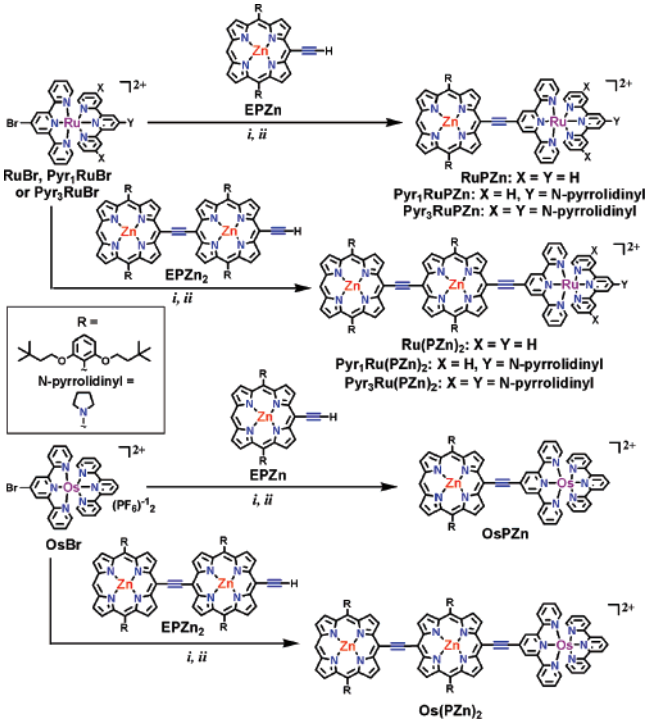

[a] Key: (i) $Pd_2(dba)_3$, $AsPh_3$, 6:3:1 MeCN−THF−TEA, 60 °C, 7 h; (ii) NH_4PF_6. R = 2′,6′-bis(3,3-dimethyl-1-butyloxy)phenyl.

Luminescent lifetimes were determined by either time-correlated, single-photon-counting (TCSPC) spectroscopy or using a streakscope-based Hamamatsu picosecond fluorescence lifetime measurement system (see below).

3. Time-Correlated, Single-Photon-Counting (TCSPC) Spectroscopy. TCSPC spectroscopic measurements were performed at the Regional Laser and Biotechnology Laboratory (RLBL) at the University of Pennsylvania using an instrument (response function = 25 ps fwhm) described previously;[52] these data were analyzed using Lifetime (RLBL) and Globals Unlimited (LFD, University of Illinois) Programs.

4. Picosecond Fluorescence Lifetime Measurement System (Streakscope). Time-resolved emission spectra were recorded using a Hamamatsu C4780 picosecond fluorescence lifetime measurement system. This system employs a Hamamatsu Streakscope C4334 as its photon-counting detector; all time delays were electronically generated by a Hamamatsu C4792-01 synchronous delay generator. The excitation light source chosen was a Hamamatsu 405 nm diode laser. All fluorescence data were acquired in single-photon-counting mode using Hamamatsu HPD-TA software. The data were analyzed using the Hamamatsu fitting module; both non-deconvoluted and deconvoluted data analyses were performed to ascertain whether or not any emissive processes were excitation pulse-limited.

5. Ultrafast Transient Absorption Experiments. The transient optical system used in this work has been discussed previously.[41] All pump−probe samples were deoxygenated via three successive freeze−pump−thaw cycles prior to measurement.

Results and Discussion

1. Synthesis. Scheme 2 outlines the syntheses of ethyne-bridged bis(terpyridyl)metal(II)−(porphinato)zinc(II) compounds **RuPZn**, **Pyr$_1$RuPZn**, **Pyr$_3$RuPZn**, **OsPZn**, **RuPZn$_2$**, **Pyr$_1$RuPZn$_2$**, **Pyr$_3$RuPZn$_2$**, and **OsPZn$_2$**; synthetic procedural details for these compounds, as well as for bis(terpyridyl)metal-

(52) Holtom, G. R. *SPIE Proc.* **1990**, *1204*, 2−12.

(II) and (porphinato)zinc(II) precursor complexes and benchmark **PZn-tpy** and **PZn$_2$-tpy** species, can be found in the Supporting Information. The metal-mediated cross-coupling[53−58] of a *meso*-ethyne-functionalized (porphinato)zinc(II) species (Scheme 2) with an appropriately brominated bis(terpyridyl)-metal(II) precursor complex yields the desired supermolecular compound in high yield.

RuPZn and **OsPZn** chromophores have been synthesized by the respective cross-coupling of the 4′-brominated ruthenium or osmium bis(2,2′;6′,2″-terpyridine) complex (**RuBr** or **OsBr**) with 5-ethynyl-10,20-bis(2′,6′-bis(3,3-dimethyl-1-butyloxy)phenyl)porphinato]zinc(II) (**EPZn**) (Scheme 2).[42] **RuPZn$_2$** and **OsPZn$_2$** were prepared in a similar fashion, utilizing a *meso*-ethynylated ethyne-bridged (porphinato)zinc(II) species (**EPZn$_2$**) as the porphyrin-containing starting material (Scheme 2), while **Pyr$_1$RuPZn**, **Pyr$_3$RuPZn**, **Pyr$_1$RuPZn$_2$**, and **Pyr$_3$RuPZn$_2$** exploited appropriate pyrrolidine-bearing ruthenium bis-(terpyridyl) bis(hexafluorophosphate) reagents (**Pyr$_1$RuBr** or **Pyr$_3$RuBr**; Scheme 2). These pyrrolidine-substituted ruthenium complexes were in turn prepared by conventional synthetic methods using ruthenium trichloride as the starting material (Supporting Information). Note that while Gros reported recently the synthesis and characterization of examples of pyrrolidine-modified ruthenium(II) polypyridyl complexes,[59] because a 4,4′,4″-pyrrolidinyl-2,2′;6′,2″-terpyridine ligand (**Pyr$_3$-tpy**) was required and the 4′-chloro-2,2′;6′,2″-terpyridine precursor for 4′-pyrrolidinyl-2,2′;6′,2″-terpyridine (**Pyr$_1$-tpy**) was commercially available, an independent synthetic route was adopted (Supporting Information).

RuPZn, **OsPZn**, **RuPZn$_2$**, **OsPZn$_2$**, **Pyr$_1$RuPZn**, **Pyr$_3$RuPZn**, **Pyr$_1$RuPZn$_2$**, and **Pyr$_3$RuPZn$_2$** were isolated via column chromatography on silica using 90:9:1 CH_3CN-H_2O-saturated aqueous KNO_3 as the eluent; counterion metathesis using ammonium hexafluorophosphate followed, providing the corresponding bis(hexafluorophosphate) salts, which were used in all the spectroscopic experiments. Interestingly, while **MPZn** chromophoric benchmarks and **Pyr$_m$RuPZn** derivatives have limited solubility in many common organic solvents with the exception of organonitriles and pyridines, **MPZn$_2$** and **Pyr$_m$RuPZn$_2$** species display millmolar solubilities in a wide range of organic solvents.

2. RuPZn$_2$ and OsPZn$_2$. A. Electronic Absorption Spectroscopy. The electronic absorption spectra (EAS) of **RuPZn$_2$** and **OsPZn$_2$** are displayed in Figure 1; for comparison, the previously reported[42] EAS of **RuPZn** and **OsPZn** are also plotted in this figure. Electronic absorption spectral data for all compounds are listed in Table 1. As noted previously, the EAS of **RuPZn** and **OsPZn** exhibit strong mixing of (porphinato)-zinc(II) (**PZn**) based oscillator strength with metal polypyridyl charge-resonance bands. In this regard, note that **RuPZn** and **OsPZn** electronic spectra differ markedly from the EAS characteristic of benchmark monomeric building block **EPZn** and **[M(tpy)$_2$]$^{2+}$** chromophores (see also Figure S1, Supporting

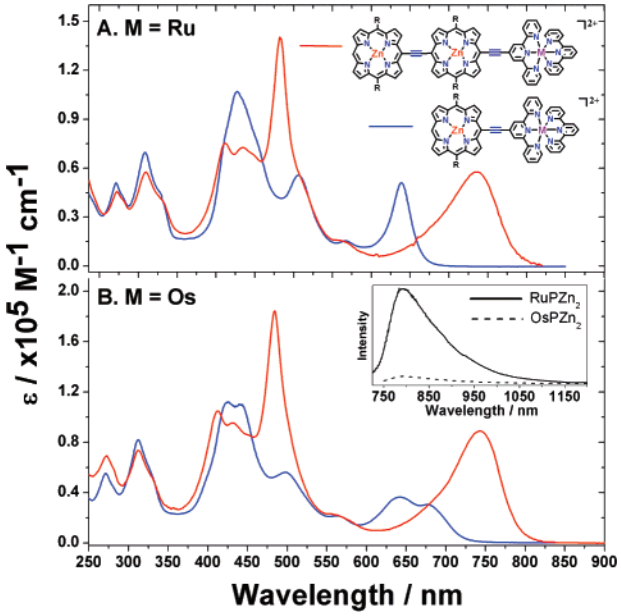

Figure 1. Comparative electronic absorption spectra of (A) **RuPZn** (solid blue line) and **RuPZn$_2$** (solid red line) and (B) **OsPZn** (solid blue line) and **OsPZn$_2$** (solid red line), in acetonitrile solvent. The inset shows the corresponding room-temperature emission spectra (λ_{exc} = 700 nm) of **RuPZn$_2$** and **OsPZn$_2$**, corrected for concentration.

Information) and do not evince transitions that derive from the simple superposition of precursor compound spectra.[42] Nevertheless, it is important to highlight that **RuPZn** and **OsPZn** absorption bands retain some spectral qualities of the transitions characteristic of classical **PZn** and **[M(tpy)$_2$]$^{2+}$** chromophores. For instance, the **RuPZn** spectrum (Figure 1A, blue line) possesses (i) two absorption bands in the ultraviolet (UV) at 272 and 309 nm, consistent with terpyridine-localized $^1\pi-\pi^*$ transitions, (ii) a very strong ($\epsilon \sim 105\,000$ M^{-1} cm^{-1}) absorption at 427 nm which exhibits significant porphyrin-derived $^1\pi-\pi^*$ Soret (B) band character, (iii) a visible band centered at 506 nm which exhibits **[Ru(tpy)$_2$]$^{2+}$**-derived singlet metal-to-ligand charge transfer (^{1}MLCT) character and features contributions from porphyrin ligand oscillator strength (vide infra), and (iv) two bands localized at 567 and 640 nm which exhibit porphyrinic $^1\pi-\pi^*$ Q-state character, with the low-energy, *x*-polarized transition manifesting features due to symmetry breaking and oscillator strength redistributions that derive from conjugation expansion[60−62] and charge resonance character that originates from the ethyne-bridged porphyrin *meso*-carbon-to-terpyridyl-4′-carbon linkage.[42] Note that to facilitate comparison of the spectral properties of these conjugated supermolecules with those of traditional (porphinato)zinc(II) and (polypyridyl)metal-(II) benchmarks, MLCT (d$-\pi^*$) and Soret- and Q-band ($\pi-\pi^*$) state and transition labels are preserved throughout this report. When these terms are used in reference to the absorption bands of **MPZn$_n$** chromophores, they denote only the dominant contributor to the oscillator strength of the transition in question; it is recognized that MLCT, ligand, Soret, and Q electronic states mix extensively in these supermolecules.[63]

(53) Heck, R. F. *Acc. Chem. Res.* **1979**, *12*, 146−151.
(54) Takahashi, S.; Kuroyama, Y.; Sonogashira, K.; Hagihara, N. *Synthesis* **1980**, 627−630.
(55) Kumada, M. *Pure Appl. Chem.* **1980**, *52*, 669−679.
(56) Negishi, E.; Luo, F. T.; Frisbee, R.; Matsushita, H. *Heterocycles* **1982**, *18*, 117−122.
(57) Stille, J. K. *Angew. Chem., Int. Ed. Engl.* **1986**, *25*, 508−523.
(58) Miyaura, N.; Suzuki, A. *Chem. Rev.* **1995**, *95*, 2457−2483.
(59) Martineau, D.; Beley, M.; Gros, P. C. *J. Org. Chem.* **2006**, *71*, 566−571.
(60) LeCours, S. M.; DiMagno, S. G.; Therien, M. J. *J. Am. Chem. Soc.* **1996**, *118*, 11854−11864.
(61) LeCours, S. M.; Guan, H. W.; DiMagno, S. G.; Wang, C. H.; Therien, M. J. *J. Am. Chem. Soc.* **1996**, *118*, 1497−1503.
(62) LeCours, S. M.; Philips, C. M.; de Paula, J. C.; Therien, M. J. *J. Am. Chem. Soc.* **1997**, *119*, 12578−12589.

Table 1. Ground-State Electronic Spectral[a] and Cyclic Voltammetric[b] Data for **RuPZn**, **OsPZn**, **RuPZn$_2$**, **OsPZn$_2$**, **Pyr$_1$RuPZn**, **Pyr$_3$RuPZn**, **Pyr$_1$RuPZn$_2$**, **Pyr$_3$RuPZn$_2$**, and Selected Chromophoric Benchmarks

	abs band max/nm (ϵ/10^5 M^{-1} cm^{-1})				potentiometric data/V	
compd	B band[c]	^{1}MLCT[c]	Q bands[c]	^{3}MLCT[c]	M^{2+}/M^{3+}	ZnP^0/ZnP^+
RuPZn[42]	427 (1.07)	506 (0.56)	567, 639 (0.15, 0.51)		1.39	0.80
OsPZn[42]	425, 440 (1.12, 1.10)	498 (0.56)	567, 642 (0.21, 0.36)	675 (0.30)	1.07	0.83
RuPZn$_2$	410, 437, 487 (0.75, 0.73, 1.40)	515 (0.52)	566, 740 (0.17, 0.57)		1.39	0.64
OsPZn$_2$	412, 434, 483 (1.05, 0.95, 1.84)	511 (0.67)	566, 740 (0.21, 0.89)	~752[d] (0.84)	1.07	0.64
Pyr$_1$RuPZn	438 (0.91)	521 (0.43)	567, 640 (0.14, 0.43)		0.99	0.80
Pyr$_3$RuPZn	439 (1.00)	528 (0.36)	566, 640 (0.15, 0.41)		0.81[e]	0.81[e]
Pyr$_1$RuPZn$_2$	411, 435, 483 (0.69, 0.66, 1.32)	526 (0.39)	566, 737 (0.15, 0.57)		1.01	0.64
Pyr$_3$RuPZn$_2$	412, 441, 483 (0.70, 0.62, 1.22)	533 (0.33)	566, 737 (0.16, 0.55)		~0.81[f]	0.64
RuBr		477 (0.15)			1.35	
OsBr		479 (0.17)		665 (0.04)	1.01	
Pyr$_1$RuBr		499 (0.19)			0.98	
Pyr$_3$RuBr		495 (0.21)			0.79	
PZn-tpy[g]	435 (2.62)		559, 604 (0.13, 0.12)			0.84
PZn$_2$-tpy[g]	408, 433, 481 (0.78, 0.79, 1.79)		556, 698 (0.15, 0.43)			0.58

[a] Spectral data were recorded in acetonitrile. "n/a" denotes transitions that were not observed. [b] Experimental conditions: [chromophore] = ~2 mM; scan rate = 0.1−0.2 V/s; reference electrode = Ag wire. $E_{1/2}$ values reported are relative to SCE; the ferrocene/ferrocenium couple (0.43 V vs SCE) was used as the internal standard. Potentiometric data for these compounds were obtained in a 0.1 M (TBA)PF_6/acetonitrile electrolyte/solvent system, except for **PZn-tpy** and **PZn$_2$-tpy**, which were interrogated in 0.1 M (TBA)PF_6/CH_2Cl_2. All reported values correspond to one electron redox couples. [c] Transition labels denote the dominant contributor to the absorption oscillator strength. [d] Estimated ^{3}MLCT absorption band λ_{max} (see text for details). [e] The Ru^{2+}/Ru^{3+} and the ZnP^0/ZnP^+ redox couples are coincident or near coincident. [f] The redox couple centered at ~0.825 V is associated with a pseudo-2e$^-$ process and is a convolution of two independent 1e$^-$ $Ru^{2+/3+}$ and $PZn^{+/2+}$ redox couples that coincidentally occur at the same voltage in this compound. The latter process appears at $E_{1/2}$ = 0.84 V in **RuPZn$_2$**, **OsPZn$_2$**, and **Pyr$_1$RuPZn$_2$**; thus, $E^{1/2}(Ru^{2+/3+})$ in **Pyr$_3$RuPZn$_2$** is estimated to be ~0.81 V. [g] Spectral data for these compounds were obtained in chloroform solvent.

OsPZn exhibits an electronic absorption spectrum similar to that observed for **RuPZn**; note that the **OsPZn** Q_x-band manifold, however, is broader [**OsPZn** Q_x(fwhm) ~900 cm^{-1}; **RuPZn** Q_x(fwhm) ~760 cm^{-1}] and exhibits an additional peak maximum (λ_{max} = 675 nm) that tails farther to the red. These spectral features derive from the larger degree of ground-state charge resonance character inherent to the osmium-containing complexes[43] and the fact that direct excitation to the ^{3}MLCT state is made possible by the larger nuclear core-charge (Z) of osmium[49] relative to that of ruthenium.

RuPZn$_2$ and **OsPZn$_2$** possess electronic absorption spectra (Figure 1) that differ markedly from those of the **RuPZn** and **OsPZn** benchmarks, although the transition assignments are largely identical. For example, the **RuPZn$_2$** EAS manifests terpyridine $^1\pi-\pi^*$ transitions and transitions dominated by porphyrin-derived Soret and Q-state character, as well as a ^{1}-MLCT-derived band that is partly obscured by the $S_0 \rightarrow S_2$ (Soret) electronic absorption manifold. Due to the extensive interpigment electronic and excitonic[64,65] interactions made possible by the *meso*-to-*meso* ethyne bridge,[26,36,37,39−41,44,66] the *x*-polarized Q-state transition manifold increases in oscillator strength relative to that observed for **RuPZn**; further, the **RuPZn$_2$** Soret band is split in a pattern characteristic of this conjugation topology, with the *x*-polarized B-bands shifted to lower energy and the *y*-polarized B-bands shifted to higher energy and broadened, reflecting the inhomogeneous distribution of structural conformers that differ with respect to the interporphyryl torsional angle.[39,41,44] As expected, the respective terpyridine $^1\pi-\pi^*$ transitions for **RuPZn** and **RuPZn$_2$** are nearly isoenergetic (Figure 1), as the ancillary terpyridine ligands (i.e., terpyridines not featuring porphyrin substitution) are essentially electronically isolated in both compounds; likewise the Q_y transitions for **RuPZn** and **RuPZn$_2$** occur at nearly the same energies, as augmented electronic delocalization afforded by an additional PZn unit and the *meso*-to-*meso* ethyne bridge in **RuPZn$_2$** exerts the greatest impact on *x*-polarized absorptions.

Note that the maximum of the **RuPZn$_2$** Q_x-band transition manifold is red-shifted by nearly 100 nm (~2135 cm^{-1}) with respect to that of the **RuPZn** benchmark; in contrast, the transition centered at ~505 nm in **RuPZn** that manifests extensive ^{1}MLCT character red-shifts a modest 9 nm (~345 cm^{-1}) in **RuPZn$_2$**. In **RuPZn** and **RuPZn$_2$**, the $\pi-\pi^*$ Q_x-band transition energy is related to the energy gap between the π-symmetric HOMO delocalized over the $(PZn\text{-ethyne})_{n=1,2}$−terpyridine framework and its corresponding LUMO having similar spatial delocalization. This $\pi-\pi^*$ energy gap differs substantially in **RuPZn** and **RuPZn$_2$** and derives in large part from the fact that $E_{1/2}(PZn^{0/+})$ is destabilized by ~160 mV in **RuPZn** relative to **RuPZn$_2$** (Table 1). On the other hand, the dominant contributor to the magnitude of the ^{1}MLCT transition energy is the energy gap between the ruthenium d-orbitals and the $(porphyrin\text{-ethyne})_{n=1,2}$ LUMO (π^*). Cyclic voltammetric measurements (Table 1) show that $E_{1/2}(Ru^{2+/3+})$ is nearly identical for **RuPZn** and **RuPZn$_2$**; thus the ^{1}MLCT transition energy depends largely on the $(PZn\text{-ethyne})_{n=1,2}$−terpyridine acceptor ligand LUMO energy in **RuPZn** and **RuPZn$_2$**. Because the magnitude of LUMO stabilization with increasing conjugation length is modest with respect to the extent of HOMO destabilization in *meso*-to-*meso* ethynyl-bridged oligomeric (porphinato)zinc(II) species (**PZn$_n$** structures),[40] the additional PZn-ethyne unit of **RuPZn$_2$** exerts a large influence on the magnitude of Q_x $\pi-\pi^*$ gap but little upon the ^{1}MLCT transition energy, relative to the analogous optical band gaps of **RuPZn** (Figure 1).

As **RuPZn** and **OsPZn** EAS are similar, so are those determined for **RuPZn$_2$** and **OsPZn$_2$** (Figure 1). As before, the

(63) For instance, the term "Q_x-state" is used to refer to the lowest energy $\pi-\pi^*$-derived transition that is polarized along the long-molecular axis in **RuPZn$_2$**, but it is understood that MLCT (d−π^*) character is mixed with this *x*-polarized absorption.

(64) McRae, E. G.; Kasha, M. The Molecular Exciton Model. In *Physical Processes in Radiation Biology, Proceedings of an International Symposium*; Augenstein, L., Mason, R., Rosenberg, B., Eds.; Academic Press: New York, 1964; pp 23−42.

(65) Kasha, M.; Rawls, H. R.; El-Bayoumi, M. A. *Pure Appl. Chem.* **1965**, *11*, 371−393.

(66) Anderson, H. L. *Inorg. Chem.* **1994**, *33*, 972−981.

only significant difference between the **RuPZn$_2$** and **OsPZn$_2$** spectra can be discerned in the low-energy absorption manifold; a ^{3}MLCT oscillator strength contribution is quasi-allowed in **OsPZn$_2$**, though this feature is obscured by the high oscillator strength Q_x-band contribution to the low-energy absorption manifold. The **RuPZn$_2$** and **OsPZn$_2$** spectra were analyzed on the basis of the assumption they are essentially identical, save for the augmented ^{3}MLCT oscillator strength in the **OsPZn$_2$** spectrum; thus, normalizing these spectra and subtracting the **RuPZn$_2$** EAS from that of **OsPZn$_2$** yields an estimate of the **OsPZn$_2$** ^{3}MLCT band position and extinction coefficient ($\lambda_{max}(S_0 \rightarrow {}^3\text{MLCT}) = 752$ nm, $\epsilon \sim 84\,000$ M^{-1} cm^{-1}) (Supporting Information, Figure S2). The energy gaps between the $S_0 \rightarrow {}^3$MLCT and $S_0 \rightarrow Q_x$ transitions for **OsPZn** and **OsPZn$_2$** are 240 and 180 cm^{-1}, respectively;[67] these data suggest that the ^{3}MLCT and Q_x $^1\pi-\pi^*$ states lay closer together in **OsPZn$_2$** than in **OsPZn**, consistent with the fact that the addition of an extra conjugated porphyrin unit to the **OsPZn** framework diminishes the Q_x $^1\pi-\pi^*$ transition energy and perturbs only slightly the energies of states possessing MLCT character, congruent with that discussed above the analogous **RuPZn** and **RuPZn$_2$** spectra. While these experiments provide no insight into the magnitude of the **RuPZn$_2$** ^{3}MLCT transition energy, the fact that bis(terpyridyl)ruthenium(II) complexes typically exhibit ^{3}MLCT energies significantly higher in energy (~2000 cm^{-1} for **[M(tpy)$_2$]$^{2+}$**)[49] than analogous bis(terpyridyl)osmium(II) complexes suggests that the **RuPZn$_2$** ^{3}MLCT state probably lies far above the Q_x-state energy; this supposition is supported by fluorescence and transient absorption data described below.[68]

B. Steady-State Fluorescence Spectroscopy. Neither **RuPZn** nor **OsPZn** exhibits observable luminescence from their respective ^{3}MLCT states at ambient or liquid-nitrogen temperatures,[42] despite the fact that the ^{3}MLCT states possess μs lifetimes at 298 K. These spectral and dynamical features are consistent with extensively delocalized T_1-state wave functions for these complexes characterized by substantial charge-separated character.[43] Such highly polarized, charge-separated **RuPZn** and **OsPZn** ^{3}MLCT states would be expected to exhibit dramatically attenuated Franck−Condon overlap relative to that manifested typically for emissive (polypyridyl)metal(II) complexes, where excited-state relaxation is dominated by charge recombination dynamics (see Supporting Information for an overview of basic **[M(tpy)$_2$]$^{2+}$** excited-state dynamics).[43]

Contrary to what is observed for the benchmark **RuPZn** and **OsPZn** complexes, **RuPZn$_2$** and **OsPZn$_2$** both exhibit observable emission bands. As depicted in the inset of Figure 1, the emission from **RuPZn$_2$** is much stronger than that of **OsPZn$_2$** (ϕ_F(**RuPZn$_2$**)/ϕ_F(**OsPZn$_2$**) ~ 12).[69] The **RuPZn$_2$** emission is weak compared to that of the precursor **PZn$_2$-tpy** compound (Supporting Information, Figure S4) and other, related *meso*-to-*meso* ethyne bridged porphyrin arrays.[41] These observed relative emission intensities are consistent with fluorescence lifetimes measured via time-correlated single-photon counting (TCSPC), of 430 and 9 ps, for **RuPZn$_2$** and **OsPZn$_2$**, respectively (Table 1). While the **RuPZn$_2$** and **OsPZn$_2$** fluorescence signatures will be discussed in more detail in the context of the ultrafast pump−probe transient absorption spectroscopic measurements below, a few points are worth noting here: (1) Given the lifetime values, the relatively small (~1040 cm^{-1}) Stokes shifts, and the spectral similarity of the appropriate transient bleach-band signal for both compounds, this emission is assigned to fluorescence ($S_1 \rightarrow S_0$) from an excited-state dominated by (porphyrin-ethyne)$_2$−terpyridine $^1\pi-\pi^*$ (Q_x) character. (2) While the $S_1 \rightarrow S_0$ λ_{max} for **PZn$_n$** chromophores shows modest solvent dependence, the emission maxima for **RuPZn$_2$** and **OsPZn$_2$** show marked solvent dependence (Supporting Information, Figure S5), with polar solvents driving larger Stokes shifts (e.g., for **RuPZn$_2$**, λ_{max}(acetonitrile) = 804 nm ($\Delta\bar{\nu}$ = 1040 cm^{-1}) and λ_{max}(toluene) = 771 nm ($\Delta\bar{\nu}$ = 525 cm^{-1})). (3) Notably, in toluene, the **RuPZn$_2$** $S_1 \rightarrow S_0$ band is significantly narrower (fwhm = 1130 cm^{-1} vs 1823 cm^{-1} in acetonitrile) and nearly 1 order of magnitude more intense than in highly polar solvents. (4) Relative to the fluorescence Stokes shifts of electronically symmetric **PZn$_n$** chromophores ($\Delta\bar{\nu} \sim 300-600$ cm^{-1}),[36,37,39−41] the Stokes shifts of **RuPZn$_2$** and **OsPZn$_2$** are significant; as the electronically asymmetric **RuPZn$_2$** and **OsPZn$_2$** $\pi-\pi^*$ states feature electronic mixing with an MLCT state and are thus more polarized, excited-state solvent relaxation plays a prominent role in determining the magnitudes of Stokes shifts and fluorescence lifetimes. In this regard, a similarly large fluorescence Stokes shift and attenuated fluorescence lifetime was observed for [(5,10,20-bis[3,5-bis(3,3-dimethyl-1-butyloxy)-phenyl]porphinato)zinc(II)]−[(5′,15′-ethynyl-10′,20′-bis[10,20-bis(heptafluoropropyl)porphinato)zinc(II)]ethyne, an electronically asymmetric *meso*-to-*meso* ethyne-bridged bis[(porphinato)-zinc(II)] complex,[39] in which the Q_x absorption manifold features a significant charge resonance contribution.

C. Femtosecond Pump−Probe Transient Absorption Spectroscopy of RuPZn and OsPZn. The early time-delay transient absorption spectra of **RuPZn** and **OsPZn** share several common features. These include (i) weak transient absorption signals in the spectral region lying between the two dominant ground-state absorption bleaching signatures and (ii) *intense* NIR transient absorption manifolds that feature extraordinary spectral breadth and enormous absorptive extinction coefficients at λ_{max}-($T_1 \rightarrow T_n$).[43] Consistent with the established spectroscopy of **[M(tpy)$_2$]$^{2+}$** and related chromophores, which have intersystem crossing times of <200 fs,[49,70−73] the intersystem crossing times of **RuPZn** and **OsPZn** are similarly fast. As such, the early time-delay ($t_{delay} \sim 360$ fs) spectra already evince characteristics of a highly polarized T_1 excited state, with the hallmark NIR absorption bands assigned as $T_1 \rightarrow T_n$. The lack of any stimulated emission ($S_1 \rightarrow S_0$) signal at even the earliest

(67) The ^{3}MLCT and Q_x states for **OsPZn$_2$** are closer in energy than the values determined from electronic absorption spectra alone would indicate. Because of the large (~980 cm^{-1}) Stokes shift for fluorescence from the Q_x state (vide infra), the Q_x-state energy is ~490 cm^{-1} closer to the ground state than as determined solely by absorption spectroscopy; this places the ^{3}MLCT ~311 cm^{-1} above the Q_x state. These relative energies are in better agreement with fluorescence and transient absorption measurements.

(68) As the **RuPZn** charge-separated triplet state is efficiently populated following electronic excitation, it must lie either below or close to the $^1\pi-\pi^*$ (Q_x) state. Given the solvent and torsional relaxation dynamics that occur on both the $^1\pi-\pi^*$ and charge-separated triplet state surfaces, the absolute state energies evolve with time; the relative state energies are thus discussed in the text only at a qualitative level.

(69) While there is a large disparity in the $S_1 \rightarrow S_0$ band intensities of **RuPZn$_2$** and **OsPZn$_2$** at room temperature, in a rigid butyronitrile glass at 77 K, the **OsPZn$_2$** band is strongly intensified (see Supporting Information, Figure S6), signifying the presence of a thermally activated quenching mechanism in **OsPZn$_2$**.

(70) Damrauer, N. H.; Cerullo, G.; Yeh, A.; Boussie, T. R.; Shank, C. V.; McCusker, J. K. *Science* **1997**, *275*, 54−57.

(71) Damrauer, N. H.; McCusker, J. K. *J. Phys. Chem. A* **1999**, *103*, 8440−8446.

(72) McCusker, J. K. *Acc. Chem. Res.* **2003**, *36*, 876−887.

(73) Bhasikuttan, A. C.; Suzuki, M.; Nakashima, S.; Okada, T *J. Am. Chem. Soc.* **2002**, *124*, 8398−8405.

observable time delays supports the conclusion that charge separation is faster than the instrument response.[43] Representative transient spectra of **RuPZn** and **OsPZn** are provided in the Supporting Information, Figure S7.

The excited-state relaxation dynamics following photoexcitation of **RuPZn** and **OsPZn** are multiexponential. **RuPZn*** and **OsPZn*** both exhibit a relaxation component with a 10−40 ps time constant, which is associated with a substantial increase in the intensity of the $T_1 \rightarrow T_n$ NIR transient absorption band. Processes on this time scale are typically assigned to structural equilibration;[39,41] the observed spectral changes in the **RuPZn** and **OsPZn** excited-state spectra indicate that the relaxed ^{3}MLCT states of these species feature conformeric distributions having a reduced mean torsional angle between the porphyrin and terpyridine least-squares planes that are more homogeneous than that for their respective initially prepared excited states.[39,41] The relaxed excited-state conformational distributions in **MPZn** species augment conjugation in the terpyridine−porphyrin π system and intensify $T_1 \rightarrow T_n$ manifold transitions (Figure S7); note that related excited-state structural dynamics are seen in simple ruthenium polypyridyl complexes that feature pyridyl ring aromatic substituents.[71,72]

While the torsional relaxation time constants determined in electronically excited **RuPZn** and **OsPZn** species are nearly identical ($\tau \sim 16$ ps), the respective associated amplitudes for these processes differ greatly. Note that the 16 ps time scale torsional relaxation process nearly doubles the $T_1 \rightarrow T_n$ transient absorption intensity for **RuPZn**; these dynamics intensify only modestly this absorption manifold in electronically excited **OsPZn** (Figure S7). These data suggest that **OsPZn** possesses a ground-state conformational distribution having a smaller average terpyridine−porphyrin interplanar torsional angle relative to **RuPZn**; this result is consistent with the facts that larger degrees of ground-state charge-transfer character and more metal−ligand bond covalency are manifest in osmium poly(pyridyl) chromophores relative to analogous ruthenium complexes.[49] In general, the fs−ps decay dynamics of **RuPZn** and **OsPZn** electronically excited states do not change appreciably as a function of excitation wavelength, indicating that higher lying π^* and CT states undergo efficient internal conversion to the charge-separated T_1 state.

D. Femtosecond Pump−Probe Transient Absorption Spectroscopy of RuPZn$_2$ and OsPZn$_2$. The transient absorption spectrum of **RuPZn$_2$** (Figure 2A, black line) in acetonitrile solvent ($\lambda_{exc} = 775$ nm; $t_{delay} \sim 300$ fs) exhibits many of the same general spectral features evident in the analogous spectrum of **RuPZn** (Figure S7); Figure 2A thus shows a transient absorption signal of moderate intensity in the visible region between the two prominent bleaching signatures and an intense NIR transient absorption feature ($\lambda_{max}(T_1 \rightarrow T_n) = 1046$ nm). In contrast to the early time delay transient absorption spectra acquired for **RuPZn**, which exhibit no stimulated emission signals, the **RuPZn$_2$** $t_{delay} \sim 300$ fs transient spectrum displays a bleaching signature due to stimulated emission, as evidenced by the negative ΔAbs contribution arising at the steady-state fluorescence spectrum (Figure 2A, dotted line) λ_{max} (~800 nm). These data suggest that the transient absorption features that characterize the early time-delay **RuPZn$_2$** spectra in Figure 2A derive in large part from a low-lying electronic state that is primarily ligand localized, possessing substantial $^1\pi-\pi^*$ (Q_x) state character; as such, at short time delays, the high oscillator strength NIR absorption manifold features significant $S_1 \rightarrow S_n$ character.

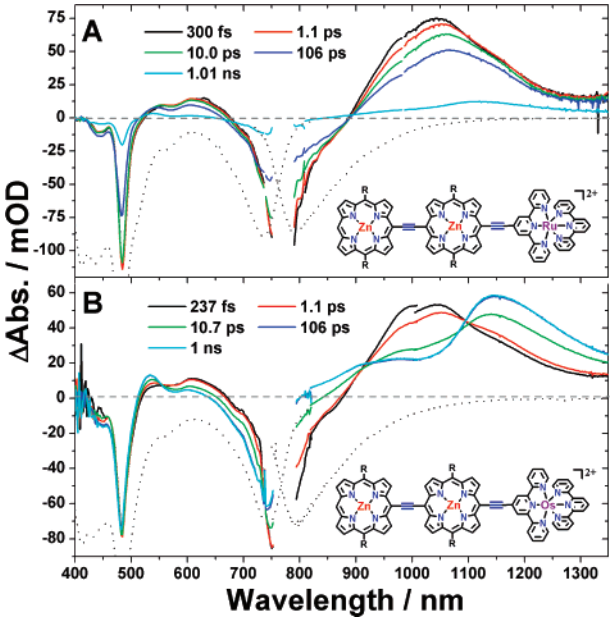

Figure 2. Pump−probe transient absorption spectra recorded at several time delays for (A) **RuPZn$_2$** and (B) **OsPZn$_2$**. Experimental conditions: solvent = acetonitrile; $\lambda_{exc} = 775$ nm; ambient temperature; magic angle polarization. R = 2′,6′-bis(3,3-dimethyl-1-butyloxy)phenyl. Scaled steady-state absorption and emission spectra (inverted dotted lines) are displayed for comparison.

Transient spectra of **RuPZn$_2$** observed at time delays >300 fs indicate that the excited-state relaxation dynamics differ significantly relative to those evinced for **RuPZn**. In electronically excited **RuPZn**, the ^{3}MLCT state populated on a sub 200 fs time scale persists well beyond the maximum time delay (~7 ns) of the transient optical system utilized for these experiments. On the other hand, the **RuPZn$_2$** excited-state spectra indicate that near-complete ground-state recovery is achieved within 7 ns after photoexcitation. In fact, in all but the longest time delays probed ($t_{delay} > 1$ ns, cyan line, Figure 2A), the spectra are characterized by stimulated emission, suggesting that the primary excited-state relaxation pathways for **RuPZn$_2$** involve either fluorescence or internal conversion (nonradiative decay) directly to the ground-state surface from a relaxed electronically excited-state dominated by (porphinato)metal−terpyridyl ligand singlet character. Note that, at $t_{delay} \sim 1$ ns, the stimulated emission signal contributes little to the transient spectrum, and a weak red-shifted NIR transient absorption band is evident, indicating a low quantum yield conversion to excited states having higher spin multiplicity. Given the similarity of the **RuPZn$_2$** excited-state spectral evolution with that determined for *meso*-to-*meso* ethyne bridged (porphinato)zinc(II) (**PZn$_n$**) arrays,[39,41] the red-shifted, low oscillator strength NIR transient absorption manifold evident at long time delays arises likely from ligand-localized $T_1 \rightarrow T_n$ transitions.

Quantitatively, the dynamics of the **RuPZn$_2$** NIR $S_1 \rightarrow S_n$ transition spectral evolution can be fit to a function of four exponentials, with time constants and associated amplitudes of $\tau_1 = 974$ ps ($A = 9.5$), $\tau_2 = 244$ ps ($A = 55.2$), $\tau_3 = 10.4$ ps ($A = -14.3$), and $\tau_4 = 3.4$ ps ($A = 17.7$). τ_1 and τ_2 contribute to ground-state recovery ($\tau_{avg} \sim 351$ ps) and are assigned to the intrinsic singlet-state lifetime, in close agreement with the

Table 2. Excited-State Electronic Spectral Data[a] for **RuPZn**, **OsPZn**, **$RuPZn_2$**, **$OsPZn_2$**, **Pyr_1RuPZn**, **Pyr_3RuPZn**, **Pyr_1RuPZn_2**, and **Pyr_3RuPZn_2**

compd	$\lambda_{max}(S_1 \rightarrow S_n)$[b]/nm	$\lambda_{max}(T_1 \rightarrow T_n)$[b]/nm ($\epsilon_e/10^5$ M^{-1} cm^{-1})[c]	τ_{CS}[b]/ps	τ_{CR}[d]/μs	τ_F[e]/ps	$\lambda_{max}(S_1 \rightarrow S_0)$/nm
RuPZn	n/a	884 (~0.30)	<0.3	44	n/a	n/a
OsPZn	n/a	964 (~0.49)	<0.3	0.86	n/a	n/a
$RuPZn_2$	1046	n/a	*f*	*f*	430	804
$OsPZn_2$	1040	1140 (~0.83)	~13	0.87	9	798
Pyr_1RuPZn	n/a	931 (~0.38)	<0.3	19.9	n/a	n/a
Pyr_3RuPZn	n/a	958 (~0.41)	<0.3	3.5	n/a	n/a
Pyr_1RuPZn_2	985	978/1122 (~0.66)	~170[g]	14.2	46.0	804
Pyr_3RuPZn_2	987	976/1126 (~0.73)	12 ± 2	6.2	12.6	805

[a] All spectral data were acquired in acetonitrile solvent. [b] $\lambda_{max}(S_1 \rightarrow S_n)$, $\lambda_{max}(T_1 \rightarrow T_n)$, and τ_{CS} values were determined using femtosecond transient absorption spectroscopy; ($\lambda_{max}(S_1 \rightarrow S_n)$ computed at $t_{delay} = 300$ fs; $\lambda_{max}(T_1 \rightarrow T_n)$ computed at $t_{delay} = 1$ ns). [c] Excited-state extinction coefficients (ϵ_e) were estimated using a method described previously.[43] No ϵ_e values were estimated for the $S_1 \rightarrow S_n$ transition due to substantial stimulated emission contributions evident at $t_{delay} = 300$ fs.[41] [d] Charge-recombination (^{3}MLCT) lifetimes were determined using ns-to-μs time-domain transient absorption measurements. [e] Fluorescence lifetimes were determined via time-correlated single photon counting (TCSPC) measurements. [f] A spectral signature for a photoinduced charge-separated state was not observed for this compound. [g] The reported 170 ps charge-separation time constant for **Pyr_1RuPZn_2** includes contributions due to structural relaxation.

fluorescence lifetime time constant ($\tau_F \sim 430$ ps, Table 2) determined by time-correlated single-photon counting (TCSPC). τ_3 and τ_4 contribute to positive and negative time-dependent ΔAbs changes for the $S_1 \rightarrow S_n$ manifold transitions as well as a slight bathochromic shift; τ_3 and τ_4 are thus assigned to structural and solvent relaxation processes, respectively. The excited-state spectra and dynamics are relatively insensitive to the excitation wavelength (Supporting Information, Figure S8), although the excited-state relaxation dynamics following excitation on the high-energy side of the lowest energy electronic absorption band λ_{max} ($\lambda_{exc} = 690$ nm) are characterized by larger amplitude spectral changes associated with structural relaxation processes than those that occur following 775 nm excitation. This derives from the fact that optical pumping at 690 nm preferentially excites a distribution of ground-state conformers featuring relatively large porphyrin−terpyridine torsional angles, whereas excitation at 775 nm interrogates a conformeric distribution characterized by a smaller mean (porphinato)zinc−terpyridyl torsional angle, which resembles more closely the relaxed excited-state conformational distribution. These data and dynamics are similar to that evinced in spectral hole-burning experiments of oligomeric **PZn_n** species.[39,41] Consistent with the observed, fast structural relaxation dynamics, **$RuPZn_2$** steady-state emission spectra are insensitive to excitation wavelength.

While the **RuPZn** and **OsPZn** excited-state relaxation dynamics are very similar, the excited-state dynamics observed for **$OsPZn_2$** offer an interesting contrast to those evinced for **$RuPZn_2$**. Representative **$OsPZn_2$** transient absorption spectra acquired in acetonitrile solvent after photoexcitation with 775 nm light are displayed in Figure 2B. Note that the early time-delay **$OsPZn_2$** spectrum ($t_{delay} \sim 300$ fs, black line) is qualitatively very similar to that of **$RuZPn_2$** (Figure 2A) and features a stimulated emission signal nearly identical with that evident in the analogous **$RuPZn_2$** spectrum. These observations support the conclusion that, at early time delays following optical excitation ($t_{delay} \sim 300$ fs), **$RuPZn_2$*** and **$OsPZn_2$*** states are similar and dominated by $^1\pi-\pi^*$ (Q_x, S_1) character; the intense NIR excited-state absorption manifold distinctive of the initially prepared **$OsPZn_2$** excited-state is thus predominantly $S_1 \rightarrow S_n$ character, as it is in **$RuPZn_2$***.

In contrast to the similarity of the **$RuPZn_2$** and **$OsPZn_2$** transient absorption spectra acquired at sub-ps time delays, the **$OsPZn_2$** pump−probe spectra recorded at time delays later than a few ps (Figure 2B) are markedly different from analogous spectra recorded for **$RuPZn_2$** (Figure 2A). Whereas the transient absorption data for **$RuPZn_2$** indicate that the excited-state complex relaxes primarily by conventional singlet-state deactivation channels (i.e., fluorescence and internal conversion), data recorded for **$OsPZn_2$*** demonstrate that the initially prepared S_1 state relaxes completely ($\tau_{avg} \sim 13$ ps, Table 2) to a new excited state (see for example spectra recorded at $t_{delay} = 10.7$ and 100 ps; Figure 2B, green and blue lines) with isosbestic behavior.[74] The electronic spectrum characteristic of this excited state exhibits the same spectral features as that evinced for the excited state probed at 300 fs time delay, except (i) the NIR transient absorption band λ_{max} is red-shifted by ~100 nm (~845 cm^{-1}) with respect to the $S_1 \rightarrow S_n$ transition λ_{max} and (ii) there is no observable stimulated emission signal in the 800−900 nm spectral region. These facts support the assignment of this new excited state as the ^{3}MLCT state, analogous to the charge-separated T_1 state generated after photoexcitation of the **RuPZn** and **OsPZn** benchmarks. Note that this state persists beyond $t_{delay} \sim 7$ ns and that the formation of the state occurs with almost no change in the intensity of the B-band bleaching signature ($\lambda \sim 480$ nm), indicating that the quantum yield for this process approaches unity. Recall that although steady-state **$OsPZn_2$** fluorescence was observed (vide supra), the integrated **$OsPZn_2$** fluorescence intensity was more than 1 order of magnitude weaker than that of **$RuPZn_2$** and the measured **$OsPZn_2$** fluorescence lifetime ($\tau_F \sim 9$ ps) is in good agreement with the dynamics of S_1 state relaxation to the charge-separated triplet ($\tau_{cs} \sim 13$ ps).

E. Excited-State Lifetimes. While the ^{3}MLCT states of many ruthenium bis(terpyridyl) complexes are efficiently quenched by thermal population of the low-lying metal centered (^{3}MC) states (Supporting Information), the **RuPZn** excited state is long-lived in deoxygenated acetonitrile solution ($\tau \sim 44$ μs, Table 1).[43] These dynamics derive from the highly polarized, charge-separated nature of the **RuPZn** and **OsPZn** T_1 states, which causes excited-state relaxation to be determined by the charge recombination time scale. The attenuated Franck−Condon overlap of **RuPZn** and **OsPZn** ^{3}MLCT states relative to those characteristic of emissive (polypyridyl)metal(II) complexes that drive these dynamics originates from the extensive LUMO

(74) The isosbestic behavior is not perfect; see spectra recorded at time delays >10 ps. This discrepancy is likely due to structural relaxation processes akin to those observed in **RuPZn*** and **OsPZn*** that occur concomitant with or following the $S_1 \rightarrow {}^3$MLCT relaxation process.

Scheme 3. **RuPZn**, **OsPZn**, **$RuPZn_2$**, and **$OsPZn_2$** Jablonski Diagrams Illustrating the Relative Energetic Arrangement of Selected Electronic States and Relevant Excited-State Relaxation Processes[a]

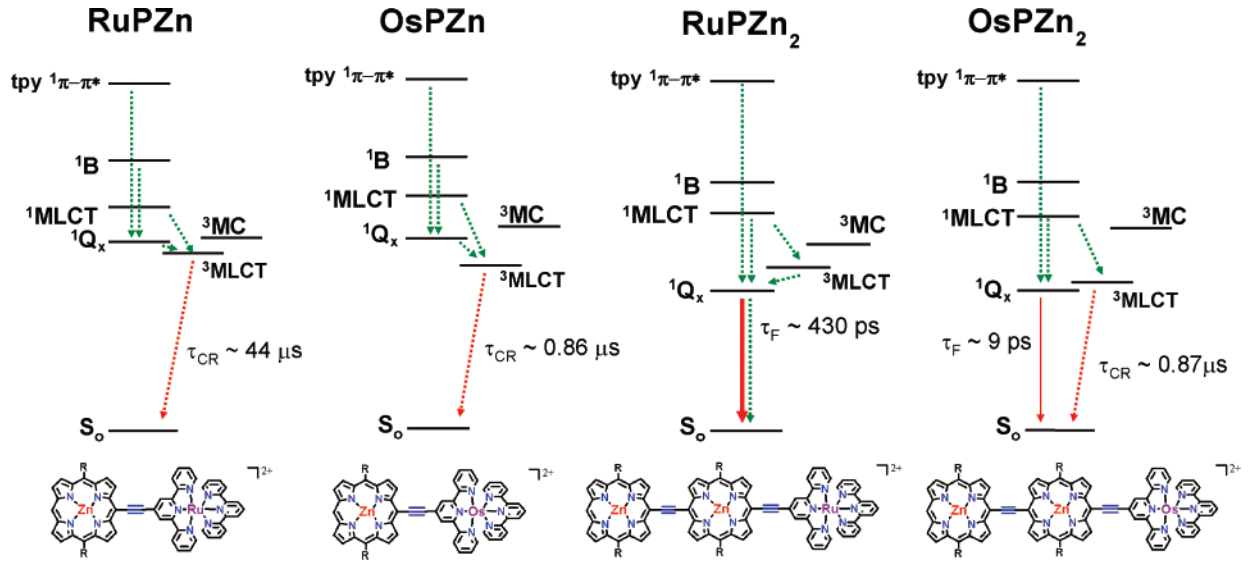

[a] State energy level separations are not to scale. Dotted green arrows represent nonradiative internal conversion and intersystem crossing processes, solid red arrows represent radiative processes (fluorescence), and dotted red arrows represent nonradiative charge-recombination (CR) processes. Measured lifetimes (τ) for relaxation of the lowest energy electronic states are indicated. Note that the ^{3}MLCT label is synonymous with the long-lived charge-separated T_1 state characteristic of many relaxed **$MPZn_n$*** species; we use this label for both brevity and emphasis of the connection of these **$MPZn_n$*** states with that of the $[Ru(tpy)_2]^{2+}$* benchmark. R = 2′,6′-bis(3,3-dimethyl-1-butyloxy)phenyl.

stabilization afforded by the conjugated (porphinato)zinc(II)−ethyne moiety. While conjugation augmentation that increases **$[Ru(tpy)_2]^{2+}$**-type ^{3}MLCT lifetimes has been demonstrated,[75] it should be emphasized, however, that the room-temperature excited-state lifetimes of such species are several orders of magnitude smaller than those elucidated for extensively delocalized, charge-separated T_1-states of **RuPZn** and **OsPZn**. The charge-separated T_1-state of **OsPZn** features a diminished lifetime ($\tau \sim 0.8$ μs, Table 1) relative to **RuPZn***, due to the increased spin−orbit coupling constant of osmium.

Oxygen efficiently quenches the ^{3}MLCT states of both compounds (Supporting Information, Figures S9A and S9G), consistent with the higher order ($S = 1$) spin multiplicities of these chromophores.[43] Congruent with the formation of a charge-separated T_1 state, the **$OsPZn_2$** excited-state lifetime is also long ($\tau \sim 0.87$ μs). While the triplet-state lifetime of **$RuPZn_2$*** was also measured ($\tau_T \sim 23$ μs), its low oscillator strength NIR transient absorption manifold evident at long time delays arises from ligand-localized $T_1 \rightarrow T_n$ transitions (vide supra) and thus is unrelated to the **RuPZn** and **$OsPZn_2$** ^{3}MLCT states which were formed at high quantum yield and feature substantial charge-separated character. The excited-state lifetimes of these compounds are listed in Table 2, and representative spectra and dynamics are plotted in the Supporting Information, Figures S9 and S10.

F. Relative State Energies for MPZn and $MPZn_2$ Chromophores. On the basis of these transient spectral data and the well-established photophysical properties of **$[M(tpy)_2]^{2+}$** complexes (see Supporting Information), a clear picture of the factors that determine whether or not a long-lived charge-separated T_1 state is formed in high yield following photoexcitation of **MPZn** and **$MPZn_2$** chromophores can be obtained; these insights are summarized in the Scheme 3 Jablonski diagrams. Note that, in Scheme 3, the ^{3}MLCT label is synonymous with the long-lived charge-separated T_1 state characteristic of many relaxed **$MPZn_n$*** species; we use this label for both brevity and to emphasize the connection of these **$MPZn_n$*** states to that of the **$[Ru(tpy)_2]^{2+}$*** benchmark. LUMO stabilization (Scheme 3) causes **$RuPZn_n$*** to feature a diminished ^{3}MLCT energy relative to **$[Ru(tpy)_2]^{2+}$*** (Scheme S6) while not impacting the energy level of the ^{3}MC state. It is well-established that the (polypyridyl)metal(II) ^{3}MC−^{3}MLCT energy gap is a dominant factor in determining the photophysical properties of these chromophores;[47−50,75−80] in **RuPZn**, because the ^{3}MLCT state lies far below the ^{3}MC energy level (Scheme 3), the lifetime of the **RuPZn** charge-separated T_1 state remains long. Relative to **RuPZn**, the ^{3}MLCT level of **OsPZn** is stabilized further, while the ^{3}MC level lies higher in energy due in large part to osmium's lower $M^{2+/3+}$ potential (Table 1); as the EAS and electrochemical data (Table 1) show that the **RuPZn** and **OsPZn** $^1\pi-\pi^*$ levels are energetically similar, quenching of the **OsPZn** ^{3}MLCT state by the higher lying ^{3}MC states is also not observed.

As described above, a long-lived ^{3}MLCT (charge-separated T_1) state of **$RuPZn_2$** is not populated appreciably at long time delays following photoexcitation. This observation stems from the fact that, in **$RuPZn_2$**, the low-lying $^1\pi-\pi^*$ (Q_x) state is stabilized dramatically but the ^{3}MLCT state energy is lowered in energy by a comparatively small degree relative to the analogous **RuPZn** state; this results in an inversion of the energetic ordering of the ^{3}MLCT and Q_x excited states, with the latter being the lower energy state in **$RuPZn_2$**. As a result,

(75) Hung, C.-Y.; Wang, T.-L.; Jang, Y. C.; Kim, W. Y.; Schmehl, R. H.; Thummel, R. P. *Inorg. Chem.* **1996**, *35*, 5953−5956.
(76) Kirchhoff, J. R.; McMillin, D. R.; Marnot, P. A.; Sauvage, J.-P. *J. Am. Chem. Soc.* **1985**, *107*, 1138−1141.
(77) Calvert, J. M.; Caspar, J. V.; Binstead, R. A.; Westmoreland, T. D.; Meyer, T. J. *J. Am. Chem. Soc.* **1982**, *104*, 6620−6627.
(78) Kober, E. M.; Marshall, J. L.; Dressick, W. J.; Sullivan, B. P.; Caspar, J. V.; Meyer, T. J. *Inorg. Chem.* **1985**, *24*, 2755−2763.
(79) Liu, D. K.; Brunschwig, B. S.; Creutz, C.; Sutin, N. *J. Am. Chem. Soc.* **1986**, *108*, 1749−1755.
(80) Hecker, C. R.; Gushurst, A. K. I.; McMillin, D. R. *Inorg. Chem.* **1991**, *30* 538−541.

the excited-state relaxation dynamics of **RuPZn$_2$** resemble those of ethyne-bridged oligomeric (porphinato)zinc(II) **PZn$_n$** arrays, with fluorescence and internal conversion being the primary pathways for excited singlet-state deactivation.[39,41] On the other hand, electronic excitation of **OsPZn$_2$** results in rapid excited-state relaxation to a long-lived charge-separated T_1 state (labeled ^{3}MLCT in Scheme 3) with near-unity quantum yield, although the process ($\tau_{CS} \sim 13$ ps) is much slower than that observed in the **MPZn** benchmarks ($\tau_{CS} < 300$ fs); note also that some fluorescence from **OsPZn$_2$*** (energetically identical with that observed from **RuPZn$_2$**) is still observed. As highlighted in the **OsPZn$_2$** EAS (Figure 1), the ^{3}MLCT and S_1 states appear to lie in close energetic proximity to one another (vide supra). Low-temperature (77 K) emission spectroscopy (Supporting Information) suggests that there is a slight thermal activation barrier for $S_1-{}^3$MLCT intersystem crossing, which is also consistent with the observed **OsPZn$_2$*** and **OsPZn*** charge-separation dynamics, underscoring that this energy gap is a primary determinant of the fate of the initially prepared excited state in these **MPZn$_n$** chromophores.

3. Pyr$_m$RuPZn and Pyr$_m$RuPZn$_2$. A. Design and Potentiometric Data. Given the excited-state dynamical properties of **RuPZn$_2$** and **OsPZn$_2$**, it is clear that further electronic modification of the **MPZn$_n$** motif is required to develop chromophores that possess the intense and wavelength-tunable NIR excited-state absorptive properties of **PZn$_n$** species, with the characteristic μs excited-state relaxation dynamics of **MPZn** chromophores. For example, further extension of the **MPZn$_2$** conjugation with additional (*meso*-ethynylporphinato)zinc(II) units would only enhance the $S_1-{}^3$MLCT energy gap and give rise to chromophores that possess nanosecond excited-state lifetimes, in which the initially prepared excited state relaxes primarily via fluorescence and nonradiative internal conversion.

Because the most significant difference between **RuPZn$_2$** and **OsPZn$_2$** complexes is the oxidation potential of the terpyridine-bound metal ion, which directly impacts the ^{3}MLCT state energy, lowering the $M^{2+/3+}$ $E_{1/2}$ value by an appropriate margin without significantly altering key π-framework orbital energy levels should drive the development of **RuPZn$_2$**-derived species in which long-lived ^{3}MLCT (charge-separated T_1) states are efficiently populated. To that end, **Pyr$_m$RuPZn$_n$** derivatives were synthesized, which feature electron-donating pyrrolidinyl groups attached to the ancillary terpyridine ligand in the 4′- (**Pyr$_1$RuPZn** and **Pyr$_1$RuPZn$_2$**) and 4,4′,4″- (**Pyr$_3$RuPZn** and **Pyr$_3$RuPZn$_2$**) positions (Chart 2). It should be noted that there is literature precedent for using dialkylamino electron-donating groups[59,81−83] to lower the ruthenium oxidation potential in (polypyridyl)ruthenium(II) complexes and, consequently, modulate ^{3}MLCT transition energies.

Potentiometric data acquired for **Pyr$_1$RuPZn, Pyr$_1$RuPZn$_2$, Pyr$_3$RuPZn**, **Pyr$_3$RuPZn$_2$**, **RuPZn**, and **RuPZn$_2$**, as well as for **RuBr**, **Pyr$_1$RuBr**, and **Pyr$_3$RuBr** building blocks, are chronicled in Table 1 (see also Supporting Information, Figure S11). These data show that the measured $Ru^{2+/3+}$ $E_{1/2}$ values decrease as pyrrolidine units are added to the ancillary terpyridyl ligand due to the augmented electron density on the ruthenium center; an increasing red-shift of the **RuBr** (660 nm), **Pyr$_1$RuBr** (709 nm), and **Pyr$_3$RuBr** (750 nm) luminescence band λ_{max} (solvent = acetonitrile, $T = 77$ K; see Supporting Information, Figure S12) is a spectroscopic manifestation of the progressively

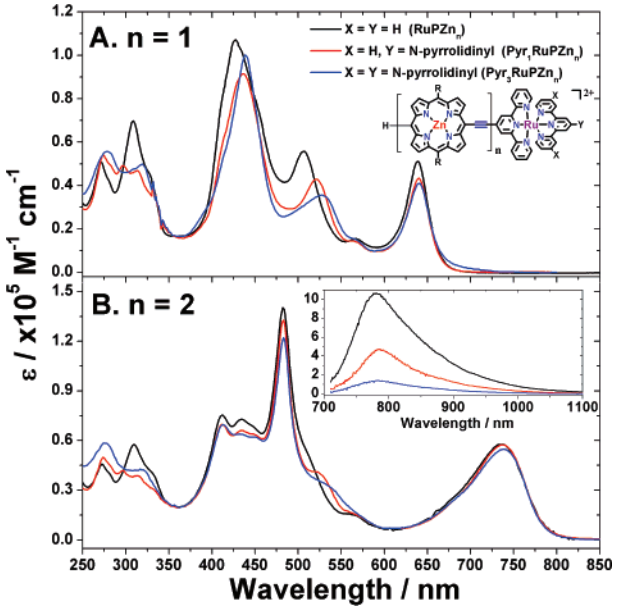

Figure 3. Comparative electronic absorption spectra of (A) **RuPZn** (black), **Pyr$_1$RuPZn** (red), and **Pyr$_3$RuPZn** (blue) and (B) **RuPZn$_2$** (black), **Pyr$_1$RuPZn$_2$** (red), and **Pyr$_3$RuPZn$_2$** (blue) recorded in acetonitrile solvent. The inset shows the corresponding emission spectra ($\lambda_{exc} = 700$ nm) of **RuPZn$_2$** (black), **Pyr$_1$RuPZn$_2$** (red), and **Pyr$_3$RuPZn$_2$** (blue) recorded at room temperature and corrected for concentration. R = 2′,6′-bis(3,3-dimethyl-1-butyloxy)phenyl.

diminishing ruthenium oxidation potential. Note that the largest $Ru^{2+/3+}$ potentiometric perturbation in this series of chromophores occurs after adding a single pyrrolidine unit, with the additional two pyrrolidines having a comparatively smaller influence [$E_{1/2}(Ru^{2+/3+})$(**RuPZn**) − $E_{1/2}(Ru^{2+/3+})$(**Pyr$_1$RuPZn**) ∼ 400 mV; $E_{1/2}(Ru^{2+/3+})$(**Pyr$_1$RuPZn**) − $E_{1/2}(Ru^{2+/3+})$(**Pyr$_3$RuPZn**) ∼ 180 mV], consistent with established effects of multiple substitution in aromatic systems.[84] Note also that there is little or no change in the measured $E_{1/2}(Ru^{2+/3+})$ value in related derivatives featuring identical degrees of pyrrolidinyl substitution [$E_{1/2}(Ru^{2+/3+})$(**Pyr$_1$RuPZn**) = 0.99 V, $E_{1/2}(Ru^{2+/3+})$-(**Pyr$_1$RuPZn$_2$**) = 1.01 V; $E_{1/2}(Ru^{2+/3+})$(**Pyr$_3$RuPZn**) = $E_{1/2}(Ru^{2+/3+})$(**Pyr$_3$RuPZn$_2$**) = 0.81 V], reflecting the weak influence of the additional (*meso*-ethynylporphinato)zinc(II) unit on the metal oxidation potential; additionally, while the ruthenium oxidation potentials change significantly as a function of the number of appended pyrrolidine units, the **PZn$_n$**-terpyridine oxidative[85] electrochemistry [$E_{1/2}(PZn^{0/+})$] is relatively unperturbed (Table 1), reflecting the fact that attenuating the metal center oxidation potential does not significantly influence the HOMO/LUMO ligand orbital energies.

B. Electronic Absorption and Fluorescence Spectroscopy of Pyr$_m$RuPZn and Pyr$_m$RuPZn$_2$ Chromophores. The comparative electronic absorption spectra of **RuPZn**, **Pyr$_1$RuPZn**, and **Pyr$_3$RuPZn** are displayed in Figure 3A, whereas the analogous spectra of **RuPZn$_2$**, **Pyr$_1$RuPZn$_2$**, and **Pyr$_3$RuPZn$_2$** are shown in Figure 3B; selected transitions are compared in

(81) Constable, E. C. *New J. Chem.* **1992**, *16*, 855.
(82) Slattery, S.; Gokaldas, N.; Mick, T.; Goldsby, K. A. *Inorg. Chem.* **1994**, *33*, 3621−3624.
(83) Hathcock, D. J.; Stone, K.; Madden, J.; Slattery, S. *Inorg. Chim. Acta* **1998**, *282*, 131−135.
(84) Hansch, C.; Leo, A.; Taft, R. W. *Chem. Rev.* **1991**, *91*, 165−195.
(85) The porphyrin−terpyridine reductive electrochemistry does not appear to change either; however, the reductive processes are in most cases irreversible; $PZn^{0/-1}$ $E_{1/2}$ values are thus not listed in Table 1.

Table 1. Comparative EAS of monomeric precursors **RuBr**, **Pyr$_1$RuBr**, and **Pyr$_3$RuBr** are provided in the Supporting Information (Figure S13). Data highlighted in the Figure 3 spectra and Table 1 data show that, in both the **Pyr$_m$RuPZn** and **Pyr$_m$RuPZn$_2$** complexes, the ^{1}MLCT transition red-shifts with increasing numbers of attached pyrrolidine groups, but the **PZn$_n$**-terpyridine derived Q_x-state ($S_0 \rightarrow {}^1\pi-\pi^*$) transition λ_{max} remains relatively unperturbed, indicating that the ^{3}MLCT states of **Pyr$_1$RuPZn$_2$** and **Pyr$_3$RuPZn$_2$** lie lower than that of **RuPZn$_2$**. Consistent with the electrochemical results, the largest change in the ^{1}MLCT energy occurs with the **RuPZn$_n$**-to-**Pyr$_1$RuPZn$_n$** electronic structural modification [λ_{max}(^{1}MLCT)(**RuPZn**) − λ_{max}(^{1}MLCT)(**Pyr$_1$RuPZn**) = 15 nm (∼570 cm^{-1}); λ_{max}(^{1}MLCT)(**RuPZn$_2$**) − λ_{max}(^{1}MLCT)(**Pyr$_1$RuPZn$_2$**) = 11 nm (∼406 cm^{-1})], with the corresponding **Pyr$_1$RuPZn$_n$**-to-**Pyr$_3$RuPZn$_n$** perturbation producing a more modest shift in this parameter [λ_{max}(^{1}MLCT)(**Pyr$_1$RuPZn**) − λ_{max}(^{1}MLCT)(**Pyr$_3$RuPZn**) = 7 nm (∼255 cm^{-1}); λ_{max}(^{1}MLCT)(**Pyr$_1$RuPZn$_2$**) − λ_{max}(^{1}MLCT)(**Pyr$_3$RuPZn$_2$**) = 7 nm (∼250 cm^{-1})].

The Figure 3 inset shows the emission spectra of **RuPZn$_2$**, **Pyr$_1$RuPZn$_2$**, and **Pyr$_3$RuPZn$_2$**, normalized for their respective absorptions at the excitation wavelength; these data demonstrate that pyrrolidine groups effect a dramatic quenching of the **Pyr$_m$RuPZn$_2$** emission intensity relative to the **RuPZn$_2$** benchmark and now resemble the corresponding normalized **OsPZn$_2$** emission spectrum (Figure 1). Insofar as the **RuPZn$_2$** emission band was assigned to fluorescence from an excited-state dominated by $^1\pi-\pi^*$ (Q_x, S_1) character due to the large energetic barrier between this and the ^{3}MLCT state (vide supra), the significant drop in fluorescence intensity in **Pyr$_1$RuPZn$_2$** and **Pyr$_3$RuPZn$_2$** relative to this benchmark is consistent with a significantly stabilized ^{3}MLCT state and efficient intersystem crossing in these pyrrolidine-derivatized chromophores.

C. Femtosecond Pump−Probe Transient Absorption Spectroscopy of Pyr$_m$RuPZn and Pyr$_m$RuPZn$_2$ Species. Analogous to the ultrafast transient absorption spectroscopic experiments described previously for **MPZn** and **MPZn$_2$** chromophores, **Pyr$_m$RuPZn** and **Pyr$_m$RuPZn$_2$** species were interrogated by pump−probe transient absorption spectroscopy. Representative transient absorption spectra at selected time delays are displayed for **Pyr$_1$RuPZn**, **Pyr$_3$RuPZn**, **Pyr$_1$RuPZn$_2$**, and **Pyr$_3$RuPZn$_2$** (Figures 4 and 5); key spectral data are highlighted in Table 2. **Pyr$_m$RuPZn** and **Pyr$_m$RuPZn$_2$** transient spectra exhibit the same absorptive and bleaching features evident in the analogous **MPZn** and **MPZn$_2$** spectra. At early time delay (t_{delay} ∼ 350 ps), **Pyr$_1$RuPZn** and **Pyr$_3$RuPZn** transient spectra (Figure 4) exhibit the hallmarks of charge-separated T_1 states (i.e., no stimulated emission signature and fast intersystem crossing to the ^{3}MLCT manifold). Note that the NIR ($T_1 \rightarrow T_n$) transition manifold λ_{max} for **Pyr$_1$RuPZn** [λ_{max}($T_1 \rightarrow T_n$) = 931 nm] and **Pyr$_3$RuPZn** [λ_{max}($T_1 \rightarrow T_n$) = 985 nm] are red-shifted (Table 2) with respect to that observed for **RuPZn** [λ_{max}($T_1 \rightarrow T_n$) = 884 nm]. The initially prepared **Pyr$_1$RuPZn** and **Pyr$_3$RuPZn** electronically excited states form the corresponding ^{3}MLCT states in the ultrafast time domain (τ_{CS} < 300 fs), similar to that observed for charge-separated T_1 state formation in the early time pump−probe spectra of the unelaborated **RuPZn*** and **OsPZn*** benchmarks; these dynamics are consistent with a ^{3}MLCT state lying well below the electronic state composed primarily of Q_x character for these

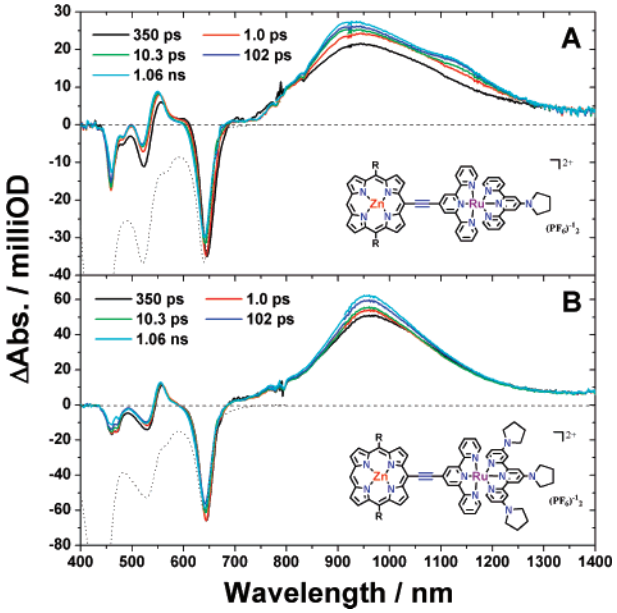

Figure 4. Pump−probe transient absorption spectra recorded at several time delays for (A) **Pyr$_1$RuPZn** and (B) **Pyr$_3$RuPZn**. Experimental conditions: solvent = acetonitrile; λ_{exc} = 775 nm; ambient temperature; magic angle polarization. Scaled steady-state absorption and emission spectra (inverted dotted lines) are displayed for comparison. R = 2′,6′-bis(3,3-dimethyl-1-butyloxy)phenyl.

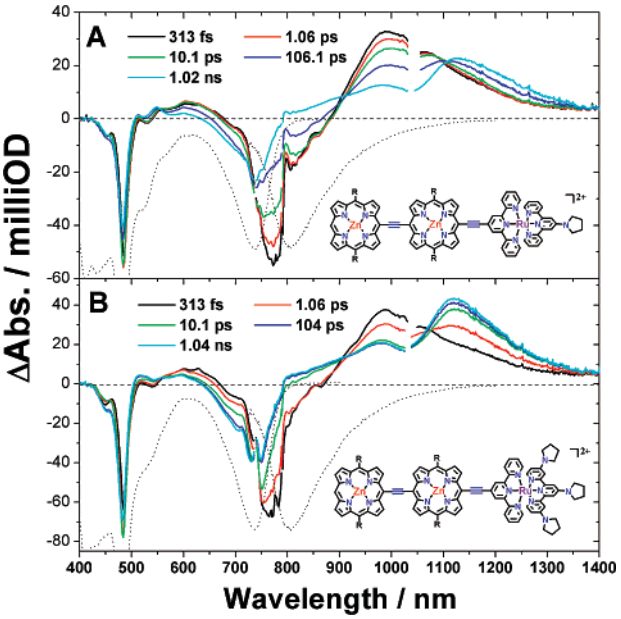

Figure 5. Pump−probe transient absorption spectra recorded at several time delays for (A) **Pyr$_1$RuPZn$_2$** and (B) **Pyr$_3$RuPZn$_2$**. Experimental conditions: solvent = acetonitrile; λ_{exc} = 775 nm; ambient temperature; magic angle polarization. Scaled steady-state absorption and emission spectra (inverted dotted lines) are displayed for comparison. R = 2′,6′-bis(3,3-dimethyl-1-butyloxy)phenyl.

species. The NIR excited-state absorption bands of both **Pyr$_1$RuPZn** and **Pyr$_3$RuPZn** exhibit extraordinary spectral breadths (∼2500 cm^{-1}) and intensities [ϵ_e @ λ_{max}($T_1 \rightarrow T_n$) ∼ 4 × 10^4 M^{-1} cm^{-1}; t_{delay} = 1 ns]. Additionally, as observed in the excited-state spectra of **RuPZn** (Figure 2), during the first 50 ps following photoexcitation, a 25−30% growth in the **Pyr$_1$RuPZn** and **Pyr$_3$RuPZn** $T_1 \rightarrow T_n$ transient absorption band intensity is manifest, consistent with structural relaxation

Scheme 4. **$RuPZn_2$**, **Pyr_1RuPZn_2**, and **Pyr_3RuPZn_2** Jablonski Diagrams Illustrating the Relative Energetic Arrangement of Selected Electronic States and Relevant Excited-State Relaxation Processes[a]

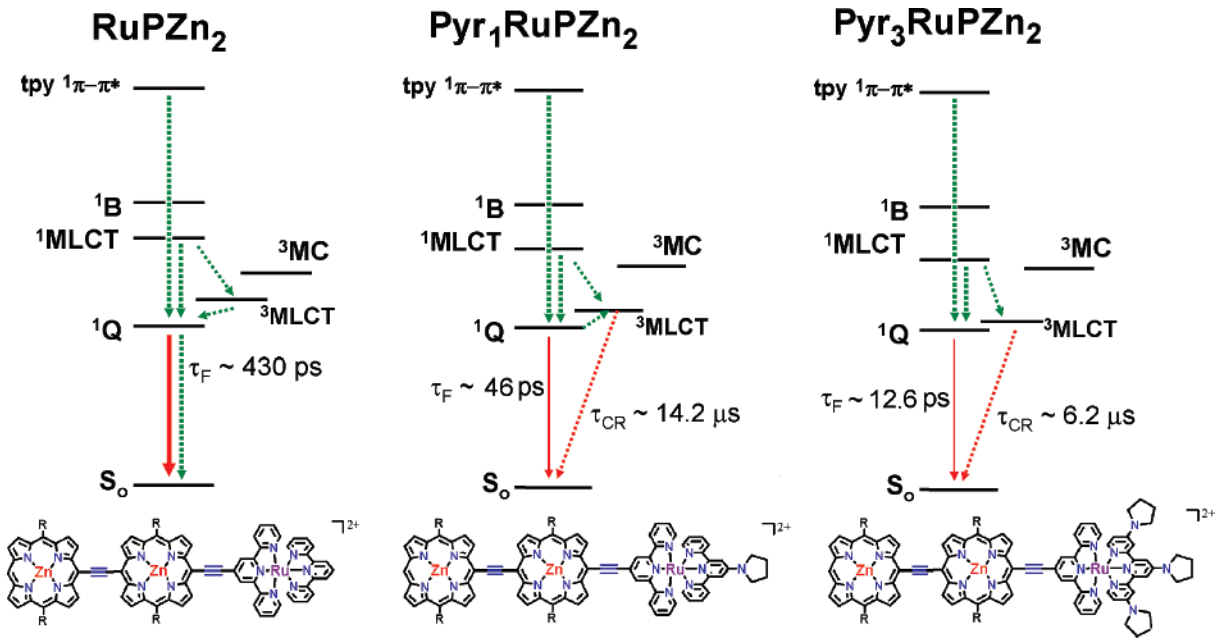

[a] State energy level separations are not to scale. Dotted green arrows represent nonradiative internal conversion and intersystem crossing processes, solid red arrows represent radiative processes (fluorescence), and dotted red arrows represent nonradiative charge-recombination (CR) processes. Measured lifetimes (τ) for relaxation of the lowest energy electronic states are indicated, as well as the respective observed emissive properties. R = 2′,6′-bis(3,3-dimethyl-1-butyloxy)phenyl.

processes that occur along the charge-separated T_1-state (^{3}MLCT) surface.

While the excited-state relaxation dynamics for **RuPZn**, **Pyr_1RuPZn**, and **Pyr_3RuPZn** are similar, the excited-state relaxation dynamics of **Pyr_1RuPZn_2** (Figure 5A) and **Pyr_3RuPZn_2** (Figure 5B) contrast those exhibited by **$RuPZn_2$**. As observed in the analogous spectrum of **$RuPZn_2$**, the **Pyr_1RuPZn_2** and **Pyr_3RuPZn_2** early time (t_{delay} ~ 350 fs) transient absorption spectra exhibit (i) strong stimulated emission signals that are coincident with their respective steady-state fluorescence spectra and (ii) intense NIR transitions centered at ~986 nm that resemble that manifest by electronically excited **PZn_2**[39] and, thus, likely feature extensive singlet character. While the nanosecond excited-state decay time scale dynamics for **$RuPZn_2$** featured ground-state recovery via fluorescence or direct internal conversion to the S_0 surface (Figure 2), the $S_1 \rightarrow S_n$ transient absorption feature characteristic of the initially prepared **Pyr_1RuPZn_2** and **Pyr_3RuPZn_2** electronically excited states decays on faster time scales (τ_{avg} ~170 and 12 ps, respectively); the decay of these transients is accompanied by the concurrent growth of a new excited-state absorptive manifold for these complexes [$\lambda_{max}(T_1 \rightarrow T_n)$(**$Pyr_1RuPZn_2$**) = 1122 nm; $\lambda_{max}(T_1 \rightarrow T_n)$(**$Pyr_3RuPZn_2$**) = 1126 nm] and the simultaneous loss of the stimulated emission signal centered at ~825 nm. The time scale for depopulation of the initially prepared excited state that features substantial singlet character is more than 1 order of magnitude faster in **Pyr_3RuPZn_2*** than in **Pyr_1RuPZn_2***, consistent with (i) the expectation that the magnitude of this time constant should track inversely with the $Q_x-{}^3$MLCT state energy gap, (ii) the fluorescence spectra determined for these complexes (Figure 3), and (iii) TCSPC spectroscopic data (Table 2).

The ^{3}MLCT lifetimes of all of these species were determined from ns−μs time scale transient absorption spectroscopy (Table 2; Supporting Information, Figure S9). Note that **Pyr_mRuPZn** and **Pyr_mRuPZn_2** species exhibit room-temperature charge-separated T_1-state lifetimes ranging from 3.5 to 20 μs, which are significantly longer than that exhibited by corresponding **OsPZn** and **$OsPZn_2$** chromophores (Table 2). Consistent with the high-spin multiplicities of the relaxed excited states of these species, appreciably reduced lifetimes are manifest in the presence of dioxygen.

D. Relative State Energies for Pyr_mRuPZn and Pyr_mRuPZn_2 Chromophores. From potentiometric data and the electronic absorption, fluorescence, and transient absorption spectroscopic experiments described above, comparative qualitative Jablonski diagrams illustrating the excited-state and relaxation dynamics of **$RuPZn_2$**, **Pyr_1RuPZn_2**, and **Pyr_3RuPZn_2** were constructed (Scheme 4). As illustrated by the analogous Jablonski diagrams for **$RuPZn_2$** and **$OsPZn_2$** displayed in Scheme 3, the dominant factor in determining the nature of the lowest lying excited state is the $S_1-{}^3$MLCT energy gap. In the **$RuPZn_2$** benchmark, the ruthenium center lies at high potential [$E_{1/2}(Ru^{2+/3+})$ = 1.39 V], leading to a relatively high-energy ^{3}MLCT state. The energy gap between the low-lying excited state composed predominantly of Q_x (S_1) character and the ^{3}MLCT level is large with respect to kT at ambient temperature, and **$RuPZn_2$*** displays dynamics similar to that manifested by conventional *meso*-to-*meso* ethyne-bridged (porphinato)zinc(II) (**PZn_n**) arrays (high quantum yield $S_1 \rightarrow S_0$ fluorescence, $S_1 \rightarrow S_0$ internal conversion, and low quantum yield $S_1 \rightarrow T_1$ intersystem crossing).[39,41] In contrast, **Pyr_3RuPZn_2** possesses a much lower potential metal terpyridyl center ($E_{1/2}(Ru^{2+/3+})$ = 0.81 V), which diminishes its corresponding ^{3}MLCT state energy. Due to potentiometric and spectroscopic properties described previously, the Q_x states of **$RuPZn_2$** and **Pyr_3RuPZn_2** are nearly isoenergetic; **Pyr_3RuPZn_2** thus possesses a low-energy ^{3}MLCT state, making possible the light-driven produc-

tion of a charge-separated T_1 state in which the time scale for ground-state recovery lies in the microsecond regime and is determined by charge-recombination dynamics. Note that **Pyr$_1$RuPZn$_2$** exhibits relaxation dynamics midway between those discussed for **RuPZn$_2$** and **Pyr$_3$RuPZn$_2$**. Because the **Pyr$_1$RuPZn$_2$** ruthenium center possesses an intermediate potential [$E_{1/2}(Ru^{2+/3+}) = 0.98$ V], its $S_1-{}^3$MLCT gap is diminished with respect to that for **Pyr$_1$RuPZn$_2$**; due to this modest energy gap, the **Pyr$_1$RuPZn$_2$** initially prepared excited state manifests a lower driving force for formation of a charge-separated T_1 state and thus exhibits steady-state fluorescence intensity intermediate between that observed for **RuPZn$_2$** and **Pyr$_3$RuPZn$_2$** (Figure 3).

Conclusions

A new series of chromophores, **MPZn$_n$**, which combine ethyne-bridged bis(terpyridyl)metal(II)−(porphinato)zinc(II) (**MPZn**) and oligomeric, ethyne-bridged (porphinato)zinc(II) (**PZn$_n$**) architectures, have been synthesized and characterized, along with a series of derivatives bearing pyrrolidinyl electron-releasing groups on the ancillary terpyridine units (**Pyr$_m$MPZn$_n$**). Cyclic voltammetric studies as well as NMR, electronic absorption, fluorescence, and femtosecond pump−probe transient absorption spectroscopies have been employed to study the ground- and excited-state properties of these unusual chromophores. All of these species possess intensely absorbing excited states having large spectral bandwidth that penetrate deep in the near-infrared (NIR) energy regime. Electronic structural variation of the molecular framework shows that the excited-state absorption maximum can be extensively modulated [$\lambda_{max}(T_1 \rightarrow T_n)$] (880 nm $< \lambda_{max} <$ 1126 nm), while concomitantly maintaining impressively large $T_1 \rightarrow T_n$ absorption manifold spectral bandwidth [full width at half-maximum, fwhm, ∼2000−2500 cm^{-1}]. These studies further correlate supermolecular electronic structure with the magnitude of the excited-state lifetime (τ_{es}) and demonstrate that this parameter can be modulated extraordinarily over 4 orders of magnitude (∼1 ns $< \tau_{es} <$ 45 μs).

This work highlights that (i) coupled oscillator photophysics and metal-mediated cross-coupling reactions can be exploited to create highly conjugated (polypyridyl)metal(II)−(porphinato)-zinc(II) supermolecules which exhibit long-lived (ns−μs time scale) excited states that feature intense absorption bands which extend deep into the near-infrared energy regime, (ii) terpyridyl pyrrolidinyl substituents can be utilized to diminish the $E_{1/2}(M^{3+/2+})$ value of the bis(terpyridyl)metal(II) center (such perturbations determine the relative energies of the **PZn$_n$**-derived $^1\pi-\pi^*$ and bis(terpyridyl)metal(II) charge-transfer states and establish whether the T_1-state wave functions of **MPZn$_n$** and **Pyr$_m$MPZn$_n$** species manifest the extensive electronic delocalization and charge-separated features characteristic of long-lived triplet states that absorb strongly in the NIR), (iii) while the excited-state dynamics and lifetimes of these complexes are unusually sensitive to the magnitude of the $S_1-{}^3$MLCT energy gap that is controlled by the pyrrolidinyl substitution, **Pyr$_m$MPZn$_n$** compounds possess ground-state absorptive properties that are nearly identical with their respective **MPZn$_n$** benchmarks, and (iv) because this new class of chromophores possess many properties (μs excited-state lifetimes, solubility in a wide range of organic solvents, highly polarized low-energy excited states, and extremely large ground-state and excited-state molar absorptivities over large, technologically important wavelength windows) that have heretofore been without precedent in single chromophoric entities, **Pyr$_m$MPZn$_n$** compounds and related structures may find unique utility in a wide range of optoelectronic applications.

Acknowledgment. This work was supported by a grant from the Department of Energy (DE-FG02-04ER46156). T.V.D respectfully acknowledges a Carolyn Hoff Lynch Graduate Fellowship, and T.I. gratefully thanks the Japan Society for the Promotion of Science (JSPS) for a postdoctoral fellowship. We acknowledge the MRSEC and NSEC programs of the National Science Foundation for infrastructural support and express their gratitude to Dr. Thomas Troxler, Dr. Louise E. Sinks, and Mr. Ian Stanton at the University of Pennsylvania for fluorescence lifetime measurements.

Supporting Information Available: Synthetic details and characterization data for precursor compounds, a review of metal(II)−bis(terpyridyl) photophysics, and supporting figures and schemes. This material is available free of charge via the Internet at http://pubs.acs.org.

JA0707512